Copyright Warning & Restrictions

The copyright law of the United States (Title 17, United States Code) governs the making of photocopies or other reproductions of copyrighted material.

Under certain conditions specified in the law, libraries and archives are authorized to furnish a photocopy or other reproduction. One of these specified conditions is that the photocopy or reproduction is not to be "used for any purpose other than private study, scholarship, or research." If a, user makes a request for, or later uses, a photocopy or reproduction for purposes in excess of "fair use" that user may be liable for copyright infringement,

This institution reserves the right to refuse to accept a copying order if, in its judgment, fulfillment of the order would involve violation of copyright law.

Please Note: The author retains the copyright while the New Jersey Institute of Technology reserves the right to distribute this thesis or dissertation

Printing note: If you do not wish to print this page, then select "Pages from: first page # to: last page #" on the print dialog screen

ABSTRACT

FAST ESTIMATION MODEL OF PRESSURE-TEMPERATURE RESPONSE FOR PLANNING FOCUSED ULTRASOUND SURGERY

by

Tariq Mohammad Arif

High Intensity Focused Ultrasound (HIFU) is becoming a widely accepted modality for extracorporeal non-invasive hyperthermia and surgical procedures. Since ultrasonic transducers need to operate in various challenging body locations, the arrangement of their array elements can be optimized to improve the capability of controlling focus intensity. In the first part of this dissertation, patterns of pressure field variations with several selected design variables (kerf, transducer element's number and element's width-height) are studied. These patterns indicate that there is a more suitable shape and arrangement of transducer elements in a specified area to achieve highest possible pressure. In order to obtain this arrangement, a Genetic Algorithm (GA) based evolutionary global search method is used to optimize the design shape and the distribution of ultrasonic transducer elements that can deliver maximum pressure at the focus zone.

This dissertation also presents a fast estimation model of focus ultrasound simulation from phased array transducer. Many simulation models have been developed to provide important information on the interactions between ultrasound beam and biological tissues as well as predictions of focused beam pattern. One of the commonly investigated issues in HIFU simulation is the calculation speed and most of the numerical models require considerable amount of time (minutes to hours) to finish one set of simulation in biological media. In the development of a fast estimation model of pressure-temperature response to support HIFU treatment planning, a numerical

simulation model, known as Rayleigh-Sommerfeld method, is used. As the Rayleigh-Sommerfeld method is applicable only with homogenous media, a modified computation method that can deal with scattering and refractions from multiple tissue layers is developed to simulate the pressure field at different focus distances. A profile for prediction of maximum output pressure, power and temperature rise is then generated by using a standard Gaussian function and a Genetic Algorithm. The optimized form of prediction model function is adopted as estimation models for different tissue layers and geometric arrangements.

The average percentages of error found in homogeneous (liver) media for maximum pressure, power deposition and temperature with the fast estimation model are 0.10%, 0.20% and 0.25%, respectively, when compared with the Rayleigh-Sommerfeld method. When compared with the Angular Spectrum method, these errors are 0.50%, 1.00% and 0.77%, respectively. For heterogeneous viscera, kidney and pancreas tissues, average percentages of error in pressure estimation compared to Rayleigh-Sommerfeld method are 0.10%, 0.05% and 0.14%, respectively, and compared to Angular Spectrum method these errors are 1.83%, 1.72% and 0.76%, respectively. Average model error for maximum power deposition and temperature rise are also found to be within 1% in heterogeneous media. The methodology of this estimation model can significantly reduce the calculation time for numerical simulations. A graphical user interface program is integrated with the model to provide interactive visualization of the pressure-temperature responses at focus zone and hot spot locations.

FAST ESTIMATION MODEL OF PRESSURE-TEMPERATURE RESPONSE FOR PLANNING FOCUSED ULTRASOUND SURGERY

by
Tariq Mohammad Arif

A Dissertation
Submitted to the Faculty of
New Jersey Institute of Technology
in Partial Fulfillment of the Requirements for the Degree of
Doctor of Philosophy in Mechanical Engineering

Department of Mechanical and Industrial Engineering

August 2017

.

APPROVAL PAGE

FAST ESTIMATION MODEL OF PRESSURE-TEMPERATURE RESPONSE FOR PLANNING FOCUSED ULTRASOUND SURGERY

Tariq Mohammad Arif

Dr. Zhiming Ji, Dissertation Advisor — Date
Associate Professor of Mechanical and Industrial Engineering, NJIT

Dr. I. Joga Rao, Committee Member — Date
Professor of Mechanical and Industrial Engineering, NJIT

Dr. Pushpendra Singh, Committee Member — Date
Professor of Mechanical and Industrial Engineering, NJIT

Dr. Bernard Koplik, Committee Member — Date
Professor of Mechanical and Industrial Engineering, NJIT

Dr. Cong Wang, Committee Member — Date
Assistant Professor of Electrical and Computer Engineering, NJIT

BIOGRAPHICAL SKETCH

Author: Tariq Mohammad Arif

Degree: Doctor of Philosophy

Date: August 2017

Undergraduate and Graduate Education:

- Doctor of Philosophy in Mechanical Engineering,
  New Jersey Institute of Technology, Newark, NJ, 2017

- Master of Science in Mechanical Engineering,
  University of Tokushima, Tokushima, Japan, 2011

- Bachelor of Science in Mechanical Engineering,
  Bangladesh University of Engineering and Technology, Dhaka, Bangladesh, 2005

Major: Mechanical Engineering

Presentations and Publications:

Tariq M. Arif and Zhiming Ji, "Fast Estimation Model of Maximum Pressure-Temperature Response for Planning Focused Ultrasound Surgery", (Submitted to Computer Methods in Biomechanics and Biomedical Engineering)

Tariq M. Arif and Zhiming Ji, "Phased Array Element Optimization of Trans-Rectal Focus Ultrasound Transducer by Evolutionary Algorithm", (In preparation)

Tariq M. Arif and Zhiming Ji, "Design Optimization of Ultrasonic Transducer Element by Evolutionary Algorithm", Proceedings of ASME 2014 International Mechanical Engineering Congress and Exposition, Vol.11: Systems, Design, and Complexity, Canada, Nov 2014.

Teruaki Ito, M. Tomotoshi and Tairq M. Arif, "A Study on Intuitive Manipulation Methods for Remote Usage of Robotic Arm", Proceedings of JSME Manufacturing Systems Division Annual Conference, Musashi University, Tokyo, 12(7): 69-70, Mar 2012.

Tariq M. Arif and Teruaki Ito, "Master-Slave Robotic Arm Manipulation for Communication Robot", Proceedings of JSME Annual Conference, Tokyo Institute of Technology, Tokyo, 11(1): S12013, Sep 2011.

Tariq M. Arif and Teruaki Ito, "Implementation of Hand Gesture Interface for Robotic Arm Manipulation", Proceedings of JSME Chogoku-Shikoku Branch 49th General Conference, Okayama University of Science, Okayama, 115(1): 57-58, Mar 2011.

Tariq M. Arif and Teruaki Ito, "Usability Study on Data Glove Interface for Robotic Arm Manipulation", Proceedings of JSME Kyoshu Branch Conference, University of Tokushima, Tokushima, 105(2): 127-128, Oct 2010.

Teruaki Ito and Tariq M. Arif, "Effective Use of Network Controlled Communication Robot for International Video Conference", Proceedings of Annual Conference of JSME, Nagoya Institute of Technology, Nagoya, 10(1): 3-4, Sep 2010.

Tariq M. Arif and Teruaki Ito, "Design and Manufacturing of a Face Projection Device for Communication Robot", Proceedings of JSME Chogoku-Shikoku Branch 48th General Conference, 105(1): 139-140, Hiroshima Institute of Technology, Hiroshima, March 2010.

Tariq M. Arif and Zhiming Ji, "Rapid Approach to The Determination of Rayleigh-Sommerfeld Response Field for Focused Ultrasound Simulations", Poster presented at Eleventh Annual Research Day, New Jersey Institute of Technology, Newark, NJ, Nov 2016.

In the name of Allah, Most Gracious and Most Merciful.

This thesis is dedicated,

To my parents: Fazilatun Nessa and Imdad Hossain Lutfi
To my family members: Mahbuba Sultana, Jinia Akter,
Khalid Mohammad Sharif
and Zohan Mohammad Shahir

ACKNOWLEDGMENT

I would like to express my deepest gratitude to my dissertation advisor Dr. Zhiming Ji, for his continuous support and motivation. Without his insight and sincere guidance, this dissertation would not have been possible. His constructive advice not only have helped me to grow academically but also have a great impact on my career, and I am forever in his debt.

I would also like to thank Dr. Bernard Koplik, Dr. Pushpendra Singh, Dr. I. Joga Rao and Dr. Cong Wang, for generously serving in my dissertation committee and for their valuable feedback. I sincerely appreciate the continuous financial support that I have received from the department of Mechanical and Industrial Engineering during my doctoral studies.

I consider myself very lucky to have some wonderful friends and colleagues at NJIT. They have always given me technical support, motivation and advice. I want to take this opportunity to thank Dr. Herli Surjanhata, Dr. Swapnil Moon and Dr. MD Shahadat Hossian from Mechanical and Industrial Engineering Department, and Dr. Md Nasir Uddin Bhuyian from Electrical and Computer Engineering Department.

Finally, I would like to thank my family members especially my father, Imdad Hossain Lutfi; my mother, Fazilatun Nessa; my brother, Khalid Mohammad Sharif; and my wife, Mahbuba Sultana for filling my life with love and enthusiasm.

TABLE OF CONTENTS

TABLE OF CONTENTS
(Continued)

Chapter **Page**

TABLE OF CONTENTS
(Continued)

Chapter **Page**

LIST OF TABLES

LIST OF FIGURES

LIST OF FIGURES
(Continued)

Figure **Page**

LIST OF FIGURES
(Continued)

Figure **Page**

LIST OF FIGURES
(Continued)

Figure **Page**

LIST OF SYMBOLS

α	Attenuation coefficient
ω	Excitation frequency
∂	Partial differential
ω	Excitation frequency
ρ	Density
v_0	Normal particle velocity
T	Temperature
T_a	Arterial temperature
C	Specific heat
C_b	Specific heat of blood
Q	Power deposition
w_b	Blood perfusion
f	Frequency
I_A	Acoustic intensity
k	Thermal conductivity

CHAPTER 1

INTRODUCTION

1.1 Background and Early Clinical Studies

Over the past two decades, High Intensity Focused Ultrasound (HIFU) is becoming an increasingly important modality for non-invasive surgical applications. Ultrasound beam can be focused with a high accuracy on a small volume of target tissues through the intact skin and tissue layers. This intense acoustic energy causes thermal coagulation and ablation of cells as the absorption process increases the tissue temperature. The ablation mechanism can also be achieved through cavitation process. As the vibration from ultrasonic wave causes continuous compression and rarefaction, bubbles can be produced from the released gas of the media during rarefaction. These bubbles upon collapsing have the potentiality to release high concentration of energy that create high local acoustic pressure and the propagation of shock waves (Kennedy, Ter Haar et al. 2003). In the focal area, two major effects of physical interactions between ultrasound waves and biological tissue i.e., mechanical forces and thermal heating, rapidly (within 1 second) increase tissue temperature up to 60°C or higher. Therefore, in HIFU therapy, sonication time is very critical parameter to consider. In clinical settings, to avoid boiling and gas formations, acoustic power and sonication time should be selected in such a way that tissue temperatures should not exceed 100°C (Fan and Hynynen 1996).

HIFU based hyperthermia process, which usually deals with lower temperature rises is also explored in many recent studies for possible cancerous tissue treatments. Biological studies present that 41 – 45°C temperature rise is enough to cause a direct

cytotoxic effect on cells, including the destruction of the cell membrane and cytoskeleton. Higher temperatures, above 48°C and below 100°C can induce irreversible damage to cellular proteins and vasculature which lead to tissue destruction in a very short period of time (Roemer 1999). More than 100°C temperature, superheated tissue can cause explosive localized boiling depending on the tissue types (Canney, Khokhlova et al. 2010). Usually, higher temperature is achieved through mechanical effects of focused ultrasound shock waves, and since such induced tissue necrosis replaces the uses of surgeon's scalpel, this kind of therapy is often termed as non-invasive acoustic surgery or HIFU surgery.

Although most significant advances in HIFU application have flourished over the last two decades, first demonstration of its clinical potential for the treatment of central nervous system was done during 1950s by Lindstrom (Lindstrom 1954) and Fry (Fry, Barnard et al. 1955). After that, this method was not applied in practical therapy purposes for a long time. However, in the recent years, the advancements of high power ultrasound phased array along with accurate targeting and noninvasive simulation method have made this previously suggested procedure a feasible and reliable technique for practical clinical applications. In the past few decades, HIFU treatment procedures have been explored for treating various eye conditions (Lizzi, Coleman et al. 1984) and cardiac conduction tissue ablation (Lee, Simon et al. 2000). This modality has also been widely investigated for various types of oncological conditions. A number of trials demonstrated the safety, efficacy, and feasibility of extracorporeal HIFU in the treatment of patients with hepatocellular carcinoma (HCC) (Wu, Wang et al. 2004), and these results were

verified by Kennedy et al. (Kennedy, Wu et al. 2004) and Leslie et al. (Leslie, Ritchie et al. 2012).

Several researchers have successfully implemented HIFU treatments for liver metastasis and observed minimal adverse effects (Illing, Kennedy et al. 2005, Sung, Cho et al. 2008). Breast tumor ablation has been performed using ultrasound-guided high-intensity focused ultrasound (USgHIFU) (Wu, Wang et al. 2005, Wu, Wang et al. 2007) and magnetic resonance guided high intensity focused ultrasound (MRgHIFU) (Huber, Jenne et al. 2001, Zippel and Papa 2005, Furusawa, Namba et al. 2007, Napoli, Anzidei et al. 2013). HIFU treatment for pancreatic cancer has also been tested and appears to be safe and effective for the palliation of pain (Xiong, Hwang et al. 2009). For the treatment of bone metastases, radiation therapy is currently the standard treatment procedure, and some recent clinical studies (Catane, Beck et al. 2007, Gianfelice, Gupta et al. 2008, Liberman, Gianfelice et al. 2009) suggest that HIFU based ablation can be safer and less painful option with no significant adverse events. Besides validated clinical applications of HIFU, at present a lot of clinical trials and academic research on simulation procedures are going on to facilitate different aspects of this modality.

1.2 Available Simulation Products

Several products are available to simulate focused ultrasound pressure field for both homogeneous and heterogeneous media. Some of these are commercial software and others are open source numerical codes developed by academic researchers. One of the earlier finite element commercial products for acoustic wave simulations was PZFlex (Weidlinger Associates Inc.), which is used to model the electromechanical behavior of

ultrasonic transducer (Wojcik and Abboud 1993). To calculate the pressure field, a separate module of this software, SPFlex is used (Mould, Wojcik et al. 1999). This software can create tissue maps from MRI or CT scan images and then perform focused non-linear wave propagation simulation by finite-element and explicit time-domain approach. SPFlex module is capable of solving large complex biological models. Other high-end finite element products like ANSYS and COMSOL can also simulate focused ultrasound propagation. But operating these products for therapeutic ultrasound simulation purpose requires significant user effort and computer memory. Finite element solutions usually produce more error in the nearfield region compare to their numerical model counterparts.

To address the near filed simulation problem of HIFU beam, McGough et al. (McGough 2004, McGough, Samulski et al. 2004, Kelly and McGough 2006) developed a new method known as Fast Nearfield Method (FNM) for circular, rectangle and spherical shape transducers. Several of their research studies suggest that FNM based C++ routine is more efficient than Rayleigh-Sommerfeld integral and it performs better in nearfield region than other popular numerical programs like Field II, DREAM and Ultrasim, for both time-harmonic and transient excitations.

The Rayleigh-Sommerfeld integral can be used efficiently to represent 3D pressure field from a focused ultrasound transducer. It is a popular approximation of Kirchhoff's integral formula for the Helmholtz equation (Hill 2005). In recent literature, different versions of Rayleigh-Sommerfeld integral are widely used to simulate ultrasound beam inside tissue media. Although Rayleigh-Sommerfeld approach is widely accepted method for HIFU response visualizations, it took almost hours to simulate a

time harmonic beam within a moderate tissue volume (e.g., 100 mm × 50 mm × 20 mm). To improve the calculation speed, another method known as Angular Spectrum is used, where an already calculated pressure field plane can propagate forward direction with the help of Fourier transform. Typically, Matlab based program is used for this kind of applications, since it can efficiently calculate FFT (Fast Fourier Transform) and IFFT (Inverse Fast Fourier Transform). However, for a similar calculation volume (100 mm × 50 mm × 20 mm) Angular Spectrum method may take 10 to 20 minutes to complete one simulation.

Figure 1.1 is an example of continuous wave simulation by Rayleigh-Sommerfeld method, from a transducer consisting of 32 by 4 elements with dimensions of 0.5 mm × 3 mm single element area, 0.4 mm kerf in X-Y directions and all elements focusing at 45 mm distance from the transducer surface. In this simulation, to avoid tedious calculations in nearfield region, an initial source pressure plane at a distance of wavelength/4 is used through Fast Nearfield Method (FNM). It took about 30 minutes to complete this simulation in a homogenous (water) media. Maximum pressure found for this arrangement is 4.156 MPa at the focused zone.

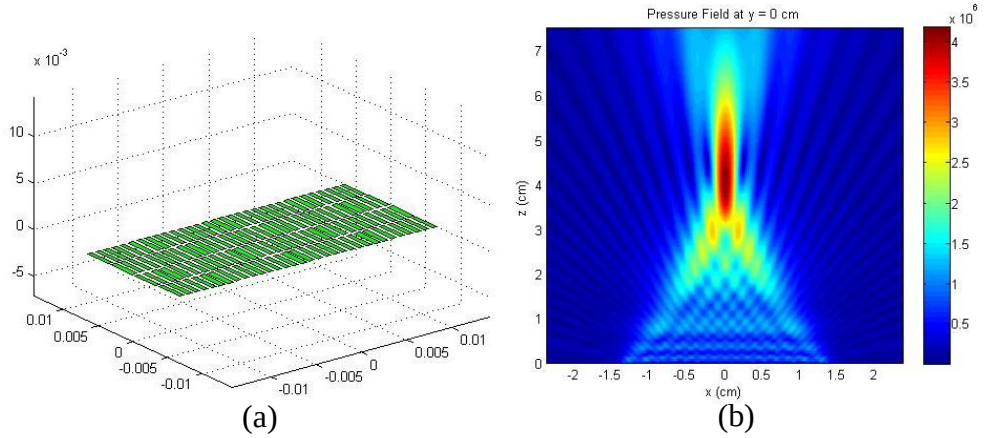

(a) (b)

Figure 1.1 (a) 32 by 4 elements transducer piston in a water media, (b) Transducer focusing 1 MHz acoustic wave at 45 mm depth.

1.3 Motivation and Approach

High intensity focused ultrasound has been used as a non-invasive surgical tool in many clinical settings including the treatment of tumors of the liver, kidney, breast, bone, uterus and pancreas, as well as conduction defects in the heart for surgical hemostasis. As ultrasound wave transmit mechanical energy using elastic properties of tissues, unlike electromagnetic waves, it does not damage tissues with ionizing radiation or accelerating electric charges. This is one of the primary reasons for ultrasound based operation to become a vital tool for non-invasive medical therapy. Since this is relatively new technology in medical surgery, simulation methods for this purpose are not as well developed as structural or mechanical simulations of other engineering scenarios. The finite element and finite difference method require considerable amount of time (minutes to hours) and computer memory to finish one session of simulation. Other well accepted numerical simulation methods like Rayleigh-Sommerfeld approach requires almost hours to finish and if factors such as tissue inhomogeneity and breathing motions are all included for more realistic simulations, processing time could take days.

Although every patient is different, their internal organs have similar arrangement inside the body. Thus, previous simulation results contain huge amount of useful information and should be explored to reduce the treatment planning time. This dissertation is aimed at developing a methodology that can make instantaneous initial predictions of pressure-temperature response based on patterns established with existing simulations results. The prediction model, while is not replacement for accurate numerical simulations, can be used to guide and reduce the sets of simulations needed for planning the treatment.

1.4 Objectives

The primary objective of this study is to support HIFU based therapy planning improvements. In this context, our suggested model is aimed to estimate HIFU field pattern and maximum pressure in the focus zone without going through complex numerical calculations. An outline of the objectives is listed here.

1. Optimize array element distribution over ultrasonic transducer piston to achieve maximum possible pressure at the focus by using Genetic Algorithm (GA).
2. Propose a fast numerical response estimation model for homogeneous tissue media.
3. Propose a fast numerical response estimation model for heterogeneous tissue media.

CHAPTER 2

TECHNICAL ASPECTS OF ACOUSTIC SURGERY

2.1 Ultrasound vs Electromagnetic Waves

The key idea of using focus ultrasound beam is to heat a deep-seated target without injuring intervening tissues. Ultrasound has the capacity to focus in a very small region, and it can safely penetrate inside human tissues better than other electromagnetic waves. For this special reason, focused ultrasound beam is widely tested in many different clinical settings in oncology, urology and neurosurgery.

In case of ultrasound hyperthermia, sound frequencies range from 500 kHz to 5 MHz is used (Roemer 1999). The mechanism of ultrasound heating can be explained by the absorption of waves and by the microscopic frictional behavior of the periodical movement of particles (Hand and James 1986). The absorption of ultrasound in biological tissue is roughly proportional to ultrasound frequency, and in water media it is proportional to the square of the ultrasound frequency. Most of the biological tissues except bone have high water content (70 to 80%), therefore a simplifying approximation that waves in the body are like waves propagating in liquids are often made during Angular Spectrum simulations. (Szabo 2014).

In case of penetration of electromagnetic waves in biological tissues, the absorption of waves found to be proportional to the medium's dielectric permittivity and conductivity (Hand and James 1986). As a wide range of electromagnetic frequencies are used in hyperthermia, the heating mechanism through this process is very challenging to explain. Typically, the radio frequency within the range of 0.1 MHz to 100 MHz, and

microwave frequency within the range of 433 MHz to 915 MHz are used during electromagnetic hyperthermia (Roemer 1999). However, the key benefits of using ultrasound over electromagnetic heating are its excellent focusing capability in a small region and its ability to target tissues deep inside the body. Ultrasound wave is also a non-ionizing radiation and it can be applied around healthy tissues multiple times if necessary.

2.2 Ultrasound Transduction Mechanism

Ultrasound transduction mechanism is based on the piezoelectric devices used to produce waves. If an electric field is applied to piezoelectric materials, their thickness changes or if a pressure pulse is applied on the surface, the imbalance of electric field of this material can lead to voltage generation (Silk 1984, Ballato 1995). The high frequency vibration of piezoelectric material by AC voltage creates ultrasonic wave that propagates through the media.

2.2.1 Piezoelectric Devices

In the early period of medical ultrasound, natural quartz crystals were used for making piezoelectric devices. But recently, they are replaced by ferroelectric ceramics such as lead zirconate titanate (PZT) with a wider band width. For ultrasound imaging applications, a higher sensitive PZT5 is used and for therapeutic focused ultrasound, low loss material PZT4 is frequently utilized (Meurant 1981, Foster, Ryan et al. 1991, Ballato 1995). These PZT materials are not ideal for making phased array transducers, since they are made by cutting grooves. Although phased array produced by PZT materials are highly efficient and capable of operating at high power, they become very brittle after

cutting grooves. Phased arrays made by PZT materials can also generate lateral vibration, which as a result may create undesirable hotspots in the treated area.

To overcome the shortcomings of PZT materials, the usability of piezocomposite materials was examined by several research groups (Chapelon, Cathignol et al. 2000, Berriet and Fleury 2007). Piezocomposite materials have predictable beam pattern, large band width with low electrical and mechanical losses. At the same time, piezocomposite materials found to be more flexible for shaping and effective manufacturing of linear or matrix arrays.

2.2.2 Capacitive Micromachined Ultrasonic Transducer (CMUT) Devices

Most of the commercial transducers are based on piezoelectricity. However, capacitive micromachined ultrasonic transducers (CMUTs), invented at Stanford University (Haller and Khuri-Yakub 1996, Soh, Ladabaum et al. 1996), during mid-1990s, have been undergoing extensive research and found to be very useful in medical imaging and HIFU therapy applications (Wong, Watkins et al. 2008, Khuri-Yakub and Oralkan 2011). CMUT's operation is based on microelectromechanical systems (MEMS) technology, and its energy transduction mechanism occurs due to the change in capacitance. CMUTs are potential competitor of piezoelectric transducers, due to ease of fabrication of complex geometries along with its bandwidth, dynamic range and sensitivity (Mills 2004). CMUT based devices is well known for making complex small shapes that may support surgical or imaging application by generating ultrasound waves. However, it is still not an accepted transduction device for HIFU surgical applications.

2.3 Transducer Geometry and Prospects of using Phased Array

Depending on the therapeutic applications ultrasound transducer geometry should be adjusted. In physiotherapies, where energy deposition near skin surface is required, plane disc transducers are used that can generate parallel beams. But, when local energy deposition is needed at a certain depth, focus beam is used. Based on the focusing method different shapes of transducers are needed. If single piezoelectric element is used, it can be shaped to form spherical focus, where geometric center of the sphere bowl is the fixed focus of that transducer. Plane transducer can be used for focusing through the uses of different shaped lenses. Focusing can also be achieved through beam steering towards focus by using multi-element phased array elements with different excitation time. Figure 2.1 shows a schematic of focusing ultrasound beam by using a phased array transducer.

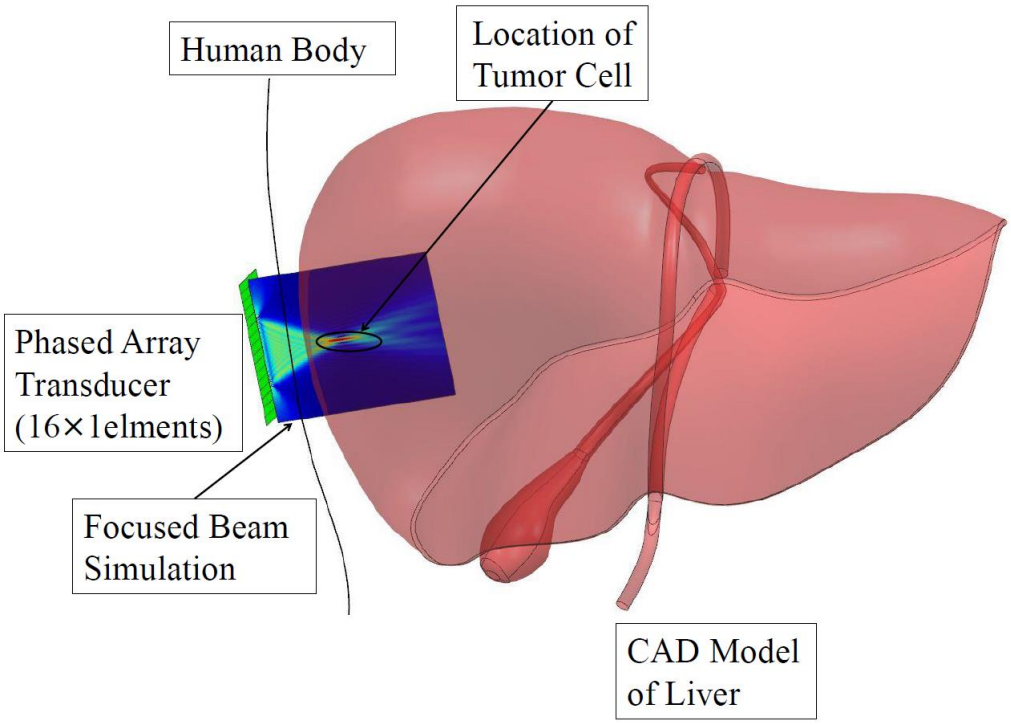

Figure 2.1 A representation of phased array transducer with 5 cm × 1 cm area and 16 × 1 array elements separated by 100 microns (kerf), focusing inside a liver model. Here, Rayleigh-Sommerfeld method is used to find output pressure field pattern over the transducer surface.

During 1990s, several researchers tried to treat local tumor hyperthermia by using single disc transducer combined with radiation therapy (Corry, Spanos et al. 1982) or single spherically curved transducer focusing multiple sonication points to cover the complete target volume (Hynynen 1991, Damianou and Hynynen 1993). At the same time, evolution of piezocomposite materials and rapid researches in this area lead to the development of phased array technology. The focusing and scanning properties of a phase array consists of rectangular transducer elements forming a section of a cylinder was developed by Ebbini et al. (Ebbini, Umemura et al. 1988). The potential performance of a phased array with non-planar geometry for deep regional hyperthermia was investigated through computer simulations by the same group (Ebbini and Cain 1991).

Although single focus high-power ultrasound beams are well known for local destruction of deep target volumes, to avoid cavitation, several closely spaced focal spots can be used to obtain a uniform temperature distribution in a larger volume (Fan and Hynynen 1995, Fan and Hynynen 1996). Fan et al. experimented with a 16 square-element phase array transducer and showed that the maximum necrosed tissue volume can be increased up to sixteen times that of a similar single element spherical transducer. When phased array is used in a non-planar geometry, the array arrangement has a natural focus at its geometric center if all the elements are driven in phase at the same time. This method compared to a planar array without geometric center, can provide higher focal intensity gain which is useful for deep penetration and heat localization. To test this idea, a 200 elements large sparse array was specially designed for trans-skull brain therapy, where randomly distributed elements were used by Pernot et al. (Pernot, Aubry et al. 2003). According to their investigation, focusing quality and performance improves when

the focus is moved by changing array element phases in the vicinity of the geometrical center. Bouchoux et al. studied another effective prototype arrangement, where an additional piezocomposite single transducer capable of obtaining high-quality image is used simultaneously with a phased array to treat deep-seated tumor (Bouchoux, Lafon et al. 2008).

CHAPTER 3

NUMERICAL SIMULATIONS

3.1 Clinical Approach

Computer simulations provide important predictions of the interactions of ultrasound beam and biological tissues. Since many of these HIFU devices are at the experimental stage, results obtained from computer simulations are highly beneficial for optimization of power depositions of prospective future medical instruments. Several popular numerical models predict diffraction of ultrasound waves, power deposition patterns and temperature distributions through computer simulations for both HIFU ablation and hyperthermia therapy applications.

In a practical clinical setting, patient models are developed by the help of anatomical images captured through Magnetic Resonance Imaging (MRI) or Computed Tomography (CT). To target the treatment area effectively, required focal position and scan paths are determined based on the geometry and position of tumor or cancerous tissue and its surroundings. Simulations determine the probable power deposition in the target area and if the treatment condition is not achieved, some parameters such as input power weights and focal points are modified to get desired results. Nonlinear effects and tissue inhomogeneities are incorporated in few of the advanced numerical models, but linear propagation models are assumed most of the time to avoid computational complexity and to reduce computation time. For a patient treatment planning, as simulations are usually repeated multiple times, speeds of these computational models are a very important factor to consider. In this chapter, several current numerical models used

for therapeutic ultrasound simulations are discussed.

3.2 Ultrasound Propagation Models

Most of the time ultrasound diffraction patterns in biological tissues are simulated by assuming a linear propagation models. These models typically calculate pressure field through Rayleigh-Sommerfeld integral or a modified version of it. A major problem associated with Rayleigh-Sommerfeld simulation is that it takes considerable amount of time. Several fast integral methods have been formulated from Rayleigh-Sommerfeld model to predict the beam pattern developed from a vibrating piston in nearfield region (Laura 1971, Kinsler 2000). An impulse response method utilizing a single integration found to be more efficient than previously used direct numerical solution approach, which requires a double numerical integration (Lockwood and Willette 1973, Arditi, Foster et al. 1981). More recently, analytical expression known as Fast Nearfield Method (FNM) was demonstrated, where near-field pressure is described by an efficient integral, that removes singularities from the impulse response and eliminate redundant calculations (McGough 2004, McGough, Samulski et al. 2004, Chen, Kelly et al. 2006, Kelly and McGough 2006). This method significantly reduces peak numerical error and computation time compared to the impulse response method or other analytical integrals.

All of these numerical models can be applied to three different transducer geometries known as rectangular piston, circular piston and spherical shell. These three kinds of transducer shapes are common in thermal therapy and predominantly considered by research groups who have developed and tested computer programs that can simulate linear or nonlinear propagation of therapeutic ultrasound. Nonlinear effects of ultrasound

propagation need to be considered when wave propagates within liquids with comparatively low acoustic attenuation, such as water, amniotic fluid or urine (Duck 2002). Nonlinear wave propagation generally include a progressive distortion of waveform and a localized change in media, which can be modeled by nonlinear wave equations, such as the Westervelt equation, the Khokhlov-Zabolotskaya-Kuznetsov (KZK) equation and the Burger's equation (Hamilton and Blackstock 1998). After getting the pressure field by simulating any of the numerical models, thermal response is calculated from that pressure field with the help of a bio-heat transfer thermal model.

The acoustic pressure field radiated from a finite transducer can be modeled with acceptable accuracy by using Rayleigh-Sommerfled integral (Goodman 1996, Kinsler 2000, Mahesh 2013). The response equation of Rayleigh-Sommerfeld integral is modified by researchers to find out pressure field for different piston shapes, such as rectangular, circular and spherical shell pistons. Using this method, time-harmonic pressure generated by an apodized rectangular source can be calculated from Equation (3.1) (Chen and McGough 2008),

$$p(x,y,z;k) = \frac{j\omega\rho v_0 e^{j\omega t}}{2\pi}\int_0^a \int_0^b f(\mu,v)\frac{e^{-jkR}}{R}d\mu dv \qquad (3.1)$$

Here, $R = \sqrt{(x-\mu)^2+(y-v)^2+z^2}$ is the distance between the source point $(\mu,v,0)$ and the observation point (x,y,z) , k is the wave number, ω is the excitation frequency, ρ is the density, v_0 is the normal particle velocity, a and b are the sides of rectangular source. The transient pressure generated with a temporal excitation component can be obtained by the inverse Fourier transform of Equation (3.1). A small rectangular element inside a

rectangular source is shown in Figure 3.1.

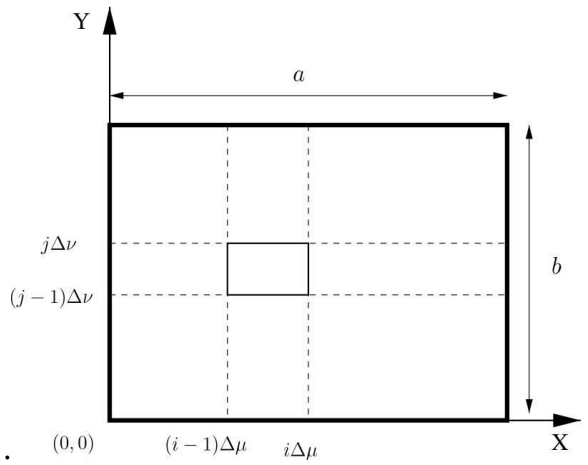

Figure 3.1 The decomposition of an apodized rectangular source into smaller rectangles, where one small rectangle is $\Delta\mu$ wide and $\Delta\nu$ high. The apodization function $f(\mu,v)$ is defined as constant over each rectangle (Chen and McGough 2008).

The Equation (3.1) can be modified to find out pressure field for rectangular, circular and spherical shell elements by using spatial impulse response method. This equation can also be utilized by using either point source superposition method or Fast Near Field Method. Further discussion on each of these methods can be found from literature references shown in Table 3.1.

Table 3.1 Literature References for Different Calculation Methods by Rectangular, Circular and Spherical Shell Geometry

References	**Array Element Geometry**		
	Rectangular	**Circular**	**Spherical Shell**
Spatial Impulse Response Method	(Lockwood and Willette 1973), (McGough 2004)	(Lockwood and Willette 1973), (Oberhettinger 1961), (Stepanishen 1971), (J. A. Archer-Hall 1979), (Hutchins, Mair et al. 1986)	(Arditi, Foster et al. 1981)
Point Source Superposition Method	(Ocheltree and Frizzel 1989), (Oberhettinger 1961), (Stepanishen 1971)	(Zemanek 1971), (Kelly and McGough 2006)	-
Fast Nearfield Method (FNM)	(McGough 2004)	(McGough, Samulski et al. 2004)	(Chen, Kelly et al. 2006, Zeng and McGough 2008)

3.3 Angular Spectrum and Fast Nearfield Method

A fast calculation method previously used in optics, known as Angular Spectrum method is used for focused ultrasound wave simulation, but it requires an initial source pressure or velocity plane. The Angular Spectrum simulation presented in this study are used for model validation purpose and these simulation results are generated by using a source pressure plane. The source plane parallel to piston surface can be calculated from analytical integral of Fast Nearfield Method (FNM) (McGough 2004), which was originally developed from the rectangular radiator method (Jensen 1999). FNM uses an increased number of samples for a higher frequency to avoid poor convergence characteristics in the nearfield region. It has been shown in several studies that by using the analytical equivalent integral of FNM expression the numerical accuracy improved in the neighborhood of the piston edge and throughout the nearfield region (McGough 2004,

McGough, Samulski et al. 2004, Chen, Kelly et al. 2006, Kelly and McGough 2006).

Once initial source pressure plane is generated at a very close distance of transducer, Angular Spectrum method can be used to develop corresponding 3D pressure field. Angular Spectrum accelerates calculations of the diffraction pattern of a wave by expanding a complex wave field into a number of parallel 2D planes (Goodman 1996). This method uses 2D Fast Fourier Transforms (FFTs) to compute the pressure field in successive planes and thus reduces the calculation time significantly than Rayleigh-Sommerfeld integral. For an efficient simulation of diffractive propagation of ultrasound beam, Angular Spectrum method is used by several researchers to predict the field profiles by transforming the spatial propagator into spatial frequency domain through 2D FFT (Christopher and Parker 1991, Dong-Lai and Waag 1997, Zemp, Tavakkoli et al. 2003). Through this method, the input pressure pattern transforms into a collection of propagating waves in the frequency domain. Again, to obtain the pressure pattern in space, the plane waves are transformed back into the space domain by using IFFT (Inverse Fast Fourier Transform). The performance of Angular Spectrum method for computing ultrasound field from a linear array transducer and its computation efficiency for single or multiple tissue layers are investigated by several researchers. Some of them developed different numerical algorithms to reduce errors and to apply this method for focused or non-focused ultrasound propagation (Orofino and Pedersen 1993, Wu, Kazys et al. 1996, Wu, Kazys et al. 1997, Clement and Hynynen 2000). Although compare to Rayleigh-Sommerfeld based calculation Angular Spectrum method is considerably faster, Rayleigh-Sommerfeld calculation is considered when simulation accuracy is the most important factor.

3.4 Thermal Model

Thermal modeling of focused ultrasound and tissue interactions is traditionally done by using the Penne's model (1948) or Penne's bio-heat transfer equation (BHTE) (Pennes 1948). This model was originally designed to predict temperature field in human forearm and it can calculate the temperature generated by local heating very effectively inside different types of tissue media. This model or its modified version was tested by many researchers as a basis of thermal treatment evaluation and become well known as "Bio-heat Transfer" model. For a transient problem, the simplified form of Penne's BHTE is given by the following equation (Moros, Roemer et al. 1988),

$$\rho C \frac{\partial T}{\partial t} + W_b C_b (T - T_a) - \nabla (k.\nabla T) = Q \qquad (3.2)$$

In Equation (3.2), T is the time dependent tissue temperature generated by power distribution Q (rate of metabolic heat source), ρ is the density, C_b is the specific heat of blood, C is the specific heat capacity, k is the thermal conductivity of tissue, W_b is the blood perfusion rate and T_a is the arterial temperature. This model does not consider several factors, such as change in blood vessel diameters, the directional dependence of perfusion heat source, varying material properties, etc.

For a steady-state problem, bio-heat transfer equation is given by Equation (3.3) (Ocheltree and Frizzell 1987).

$$-k\nabla^2 T + W_b C_b (T - T_a) = Q \tag{3.3}$$

This equation calculates the tissue temperature T for a steady-state local power deposition. The power deposition quantity used in Equation (3.2) must be optimized in order to achieve desired temperature in the focal region. Traditionally, there are several efficient optimization methods used in HIFU therapy, including a method known as pseudoinverse approach, which can precisely control over the intensity level of each of the control points in the treatment volume (Ebbini and Cain 1989). Another optimization method of power deposition, known as direct thermal inverse method, uses inverse acoustic mapping of focal requirements to find out optimal array driving signal amplitudes and phases (McGough, Ebbini et al. 1992).

CHAPTER 4

OPTIMIZATION OF ARRAY ELEMENT DISTRIBUTION

4.1 Optimization Method

When ultrasonic transducer elements focus beam on a particular region inside body, to generate pressure, surgeon needs to control temperature, frequency and exposure time according to requirements of the therapy. These factors are crucial in ultrasound surgery; therefore, various techniques have been utilized for the effective delivery of ultrasound waves. For example, focal spots are scanned along spiral trajectories under MRI guidance to achieve relatively uniform temperatures (Salomir, Palussiere et al. 2000), and superpose beam patterns with multiple foci, as this technique requires less average power and shorter time than single focus thermal dose (Daum and Hynynen 1998, Hong, Aarsvold et al. 1999). Although temperature generated in the focus point can be controlled by power input and excitation time delays of each elements, in this chapter, we are exploring the design aspect of transducers based on the element's number, dimensions and their arrangement over the surface to obtain maximum pressure field.

There are limited array arrangements found in commercially developed ultrasound transducers. If the size and arrangement of elements can be changed to increase the range of pressure by using the same transducer shape, it will provide more flexibility during therapy. When exploring the use of endoscopic approach to bring the ultrasound transducer closer to, or to open new acoustic window for, target tissue, there are many constraints on the shape and size of the transducer. We have investigated the effect of several selected transducer design variables (kerf, number, width and height of

elements) on the patterns of pressure field. To find out an optimum arrangement for a selected range of area a Genetic Algorithm based differential evolution is used together with focused ultrasound simulation to calculate pressure field and to find out the possible highest pressure at the focused zone for different arrangements of rectangular array. The optimization process is done by changing the total number of elements in X and Y direction and each element's width-height in that area. Pressures generated in each simulation are then used as an objective function for Genetic Algorithm to search for the combination of X and Y directional elements that can generate the maximum possible pressure at the focused zone. A flow of the overall procedure is shown in the Figure 4.1.

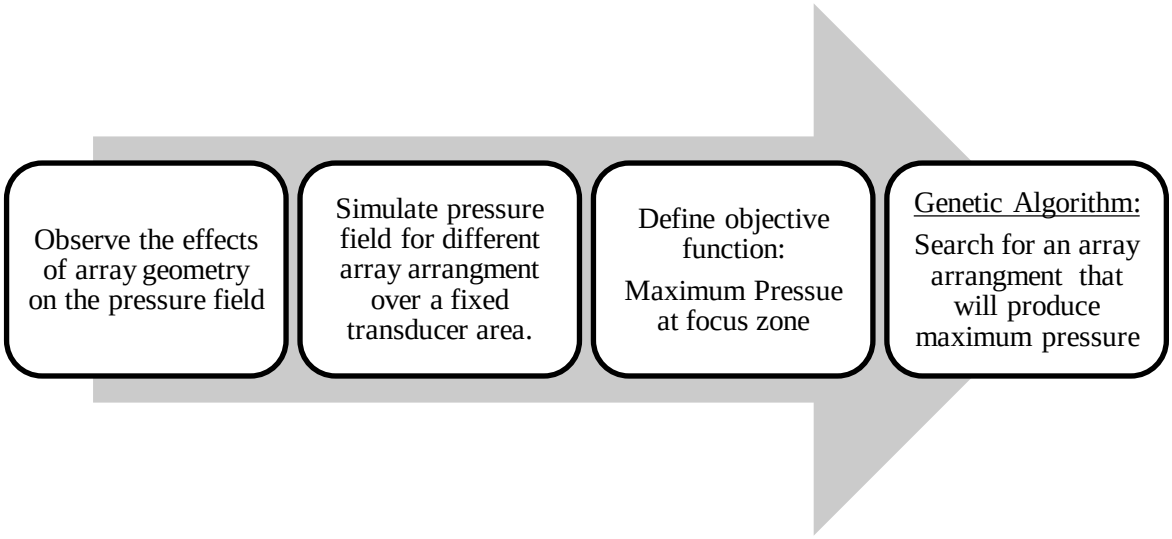

Figure 4.1 Optimization steps to find array arrangement through Genetic Algorithm.

4.2 Effects of Array Geometry on the Pressure Field

Within a given piston surface area, different transducer shape and phased array can change the intensity of pressure field during acoustic surgery. The pressure generated is directly proportional to the temperature. Based on the transducer face area, the ability to produce highest pressure field depends on several factors, such as transducer element's

area, width-height ratio, kerf, number of array elements and array distribution. We have investigated the pressure field generated in a uniform media (water) by changing several transducer design parameters for optimizing array distribution. Rayleigh-Sommerfeld simulation program for homogeneous media by FOCUS software coupled with a Genetic Algorithm is used for this optimization process. Internal tissue properties used to construct the homogeneous (water) medium are shown in Table 4.1.

Table 4.1 Parameters and Their Values in Simulation for Water Media

Parameter	***Value***
Density	1×10^3 kg/m^3
Sound Speed	1.5×10^3 m/s
Operating Frequency	1 MHz
Attenuation	0.00025 dB/cm-MHz
Specific Heat	4.180×10^3J/kg-K
Specific Heat of Blood	3.48×10^3 J/kg-K
Blood Perfusion	0 kg/m^3-s
Thermal Conductivity	6.15×10^{-1} W/m-K

For different array element dimensions, different pressure can be generated at a certain focus distance without changing input power intensity and ultrasound frequency. To check the effect of array distribution over transducer face, we have extracted maximum pressure generated from the simulation and compared it with different types of array element sizes and distributions. According to our results, geometric array distribution greatly effects the pressure field pattern as well as the maximum pressure found in that field. It has also been observed that, maximum pressure is not always found at the focused zone. For a poorly designed array distribution maximum pressure may be

found at the hot spots, which is not desirable. Figure 4.2 shows an example of pressure distribution found for a 32 by 1 array element, focusing at 3 cm distance. Here, the maximum pressure found at the focused zone is about 2.79 MPa.

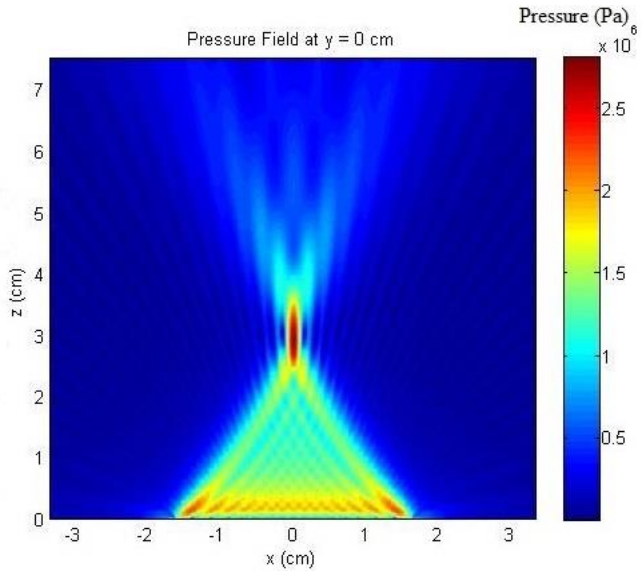

Figure 4.2 Simulated pressure field for 32 by 1 array elements (3 mm × 0.75 mm) with 100 µm kerf, focusing at 3 cm distance from transducer surface.

4.2.1 Changes of Pressure Field with Kerf

Ultrasound wave generated from a transducer is greatly affected by the space between neighboring piezoelectric elements or kerfs, since it can reduce the active area. Also, kerf effects the beam profile and side lobe levels of an array that is responsible for changing the resultant pressure field from the transducer. In this study, changes in pressure fields with variable kerf for different aspect ratio of array elements are observed through Rayleigh-Sommerfeld simulation.

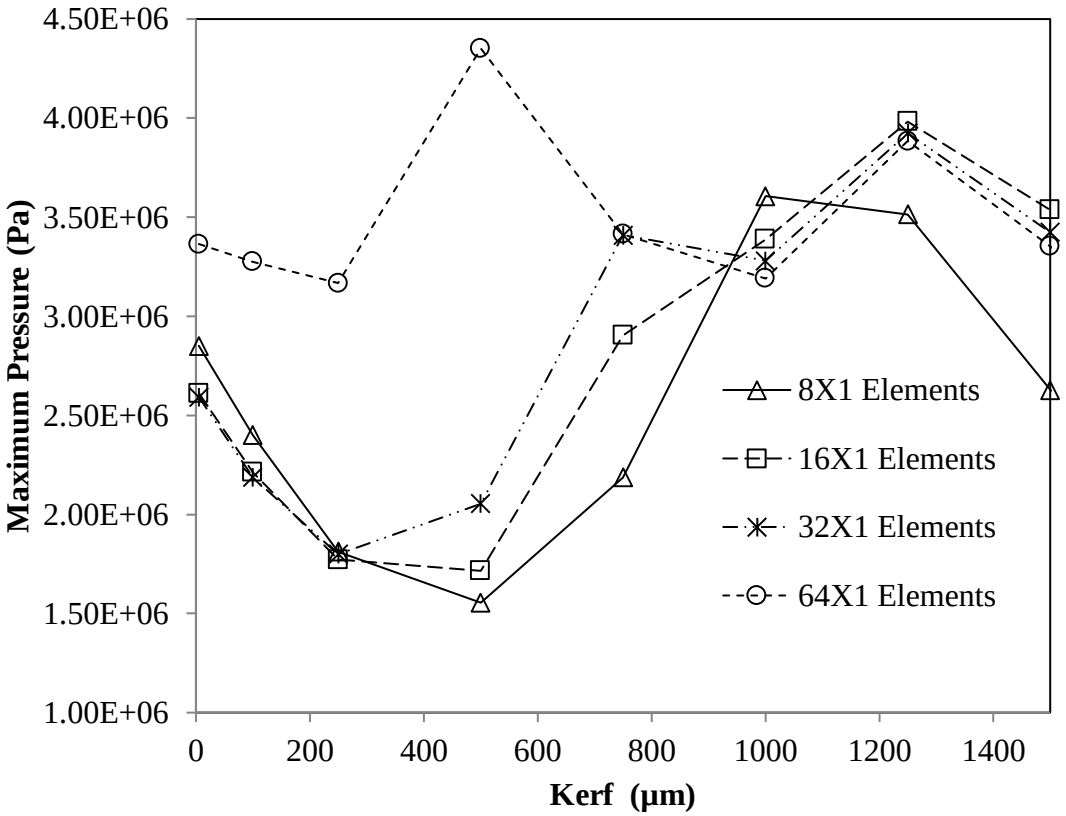

Figure 4.3 Changes of maximum pressure in simulated field within a kerf range of 5 µm to 1500 µm, for 8, 16, 32 and 64 x-elements (each element area = 0.5 mm × 4 mm) of rectangular arrays focusing at 3.75 cm distance. Here, each element's aspect ratio (height/width) is 8:1.

Figure 4.3 shows how the maximum pressure changes in between 5 µm to 1500 µm kerfs for different element numbers of array focusing at the same distance. From this figure, it is observed that for 64 × 1 elements with 500 µm kerf, maximum pressure field sharply increases and then drops again with increasing kerfs. The fluctuation in pressure filed is the result of combined effects by beam focusing from different array arrangements. Transducer elements in a linear array that are fired simultaneously produce an effective transducer width equal to the sum of the widths of the individual elements. But at the same time, individual beams interact via "constructive" and "destructive"

interference to produce a collimated beam that causes to change resultant beam profiles and maximum pressures. Since the interference is also influenced by the frequency used, the "optimal" kerf value needs to be studied for a particular frequency.

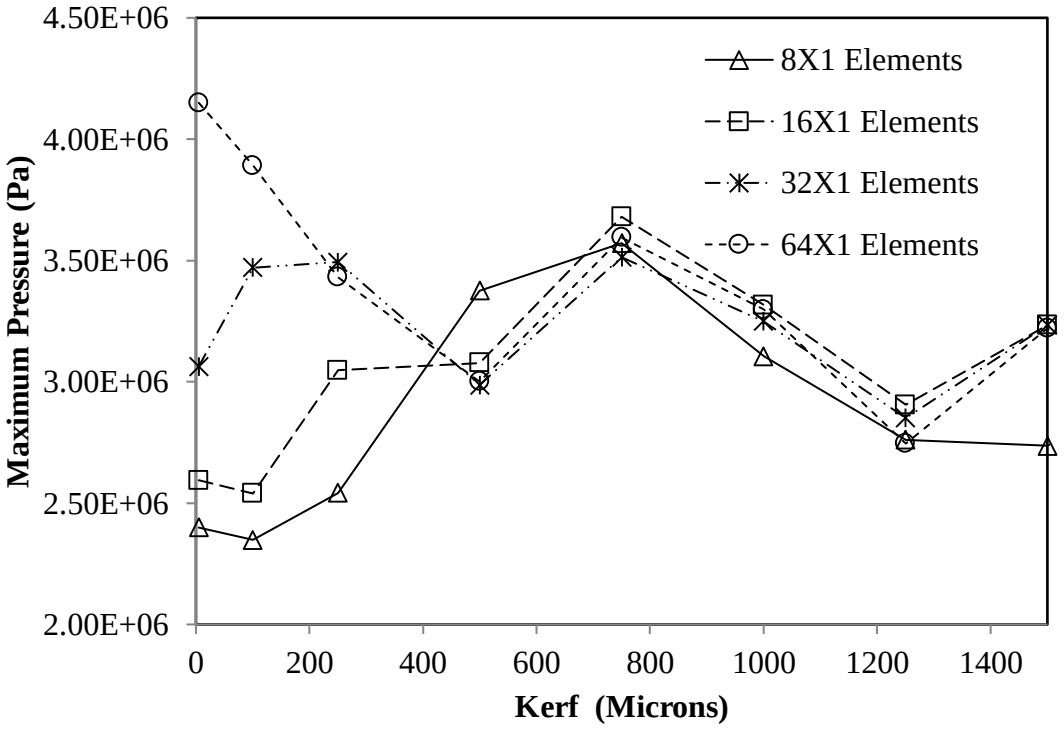

Figure 4.4 Changes of maximum pressure in simulated field within a kerf range of 5 μm to 1500 μm, for 8, 16, 32 and 64 x-elements (each element area = 1 mm × 1 mm) of rectangular arrays focusing at 3.75 cm distance. Here, each element's aspect ratio (height/width) is 1.

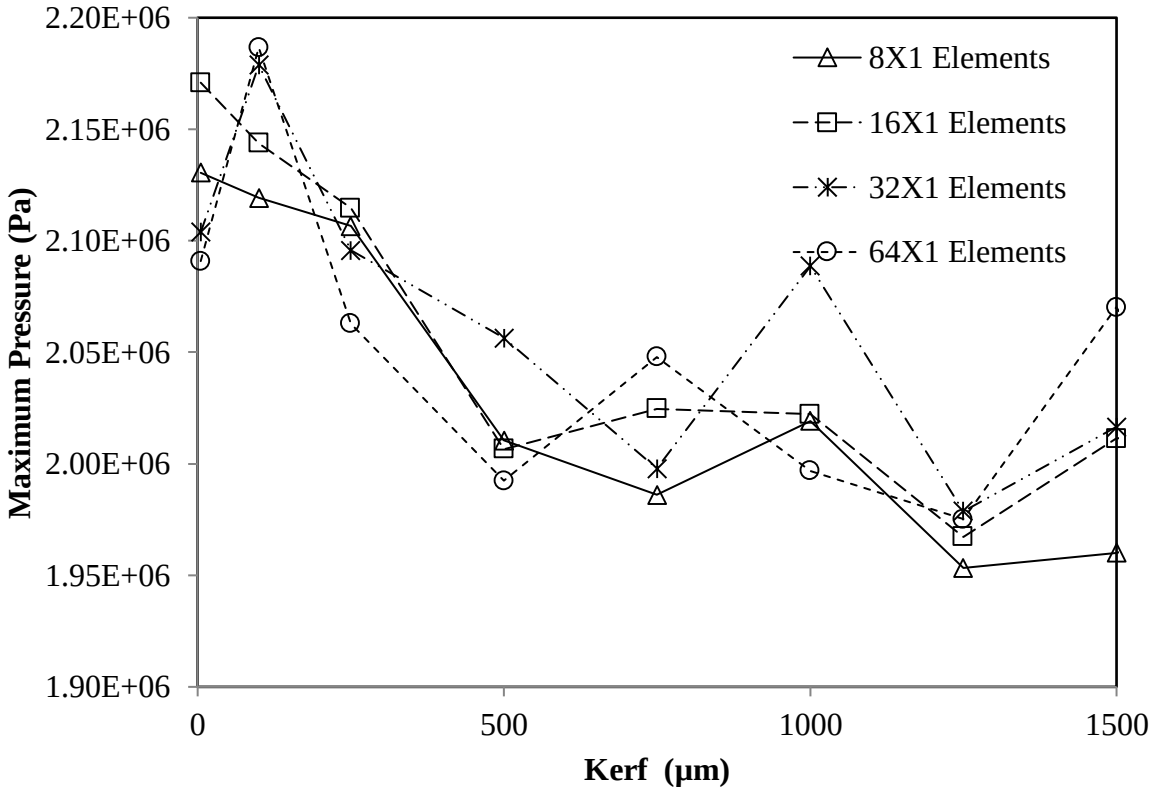

Figure 4.5 Changes of maximum pressure in simulated field within a kerf range of 5 µm to 1500 µm, for 8, 16, 32 and 64 x-elements (each element area = 4 mm × 0.5 mm) of rectangular arrays focusing at 3.75 cm distance. Here, each element's aspect ratio (height/width) is 1:8.

Figures 4.4 and 4.5 show how maximum pressure changes with kerf for different aspect ratio, forming rectangular shaped array. For cylindrical array type, maximum pressure variation with kerf for 8, 16 and 32 elements are also tested. But when more elements are used (e.g., 64 elements) maximum pressures tends to remain constant for the selected transducer geometry. In Figure 4.6, the maximum pressure variations with kerf for different cylindrical array element number have shown for elements with aspect ratio 8:1.

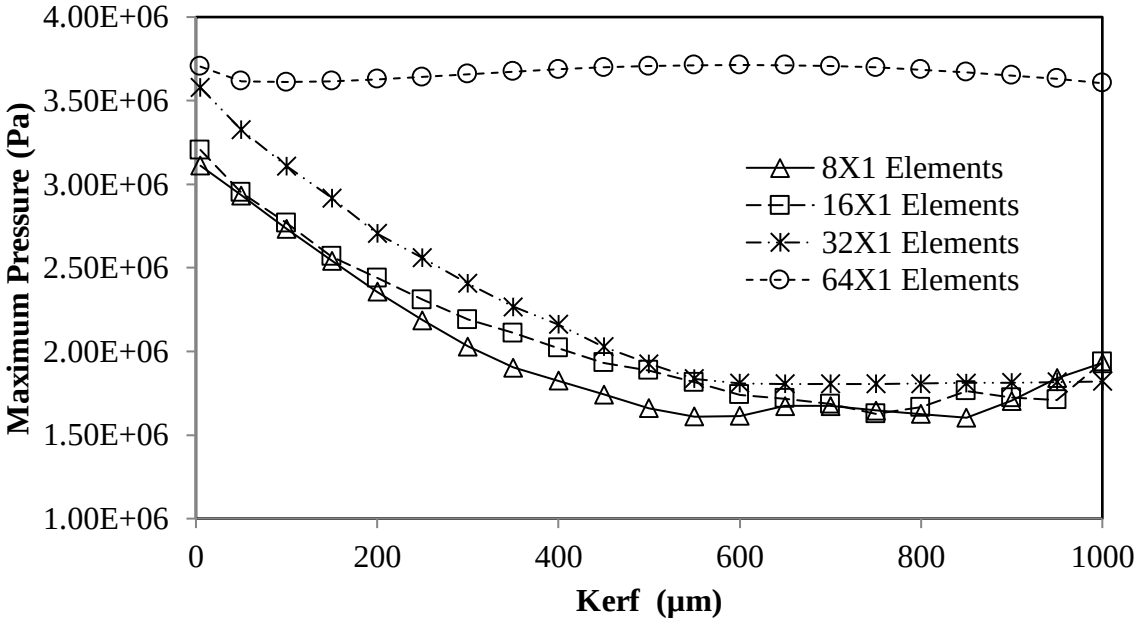

Figure 4.6 Changes in maximum pressure in simulated field within a kerf range of 5 µm to 1000 µm, for 8, 16, 32 and 64 x-elements (each element area = 0.5 mm × 4 mm) of cylindrical arrays focusing at 3.75 cm distance. Here, each element's aspect ratio (height/width) is 8:1.

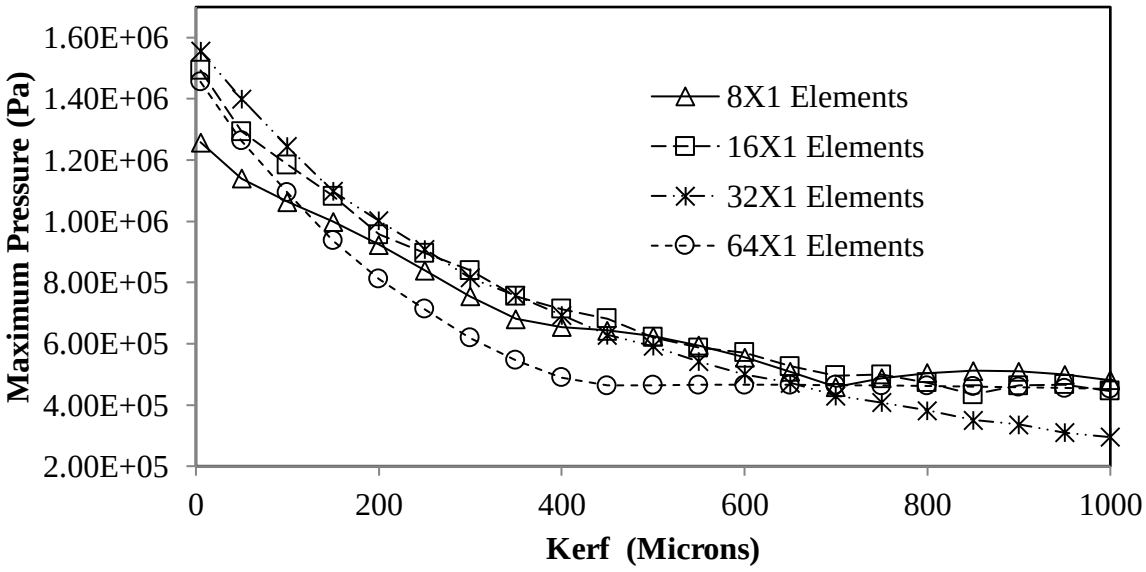

Figure 4.7 Changes in maximum pressure in simulated field within a kerf range of 5 µm to 1000 µm, for 8, 16, 32 and 64 x-elements (each element area = 0.5 mm × 0.5 mm) of cylindrical arrays focusing at 3.75 cm distance. Here, each element's aspect ratio (height/width) is 1.

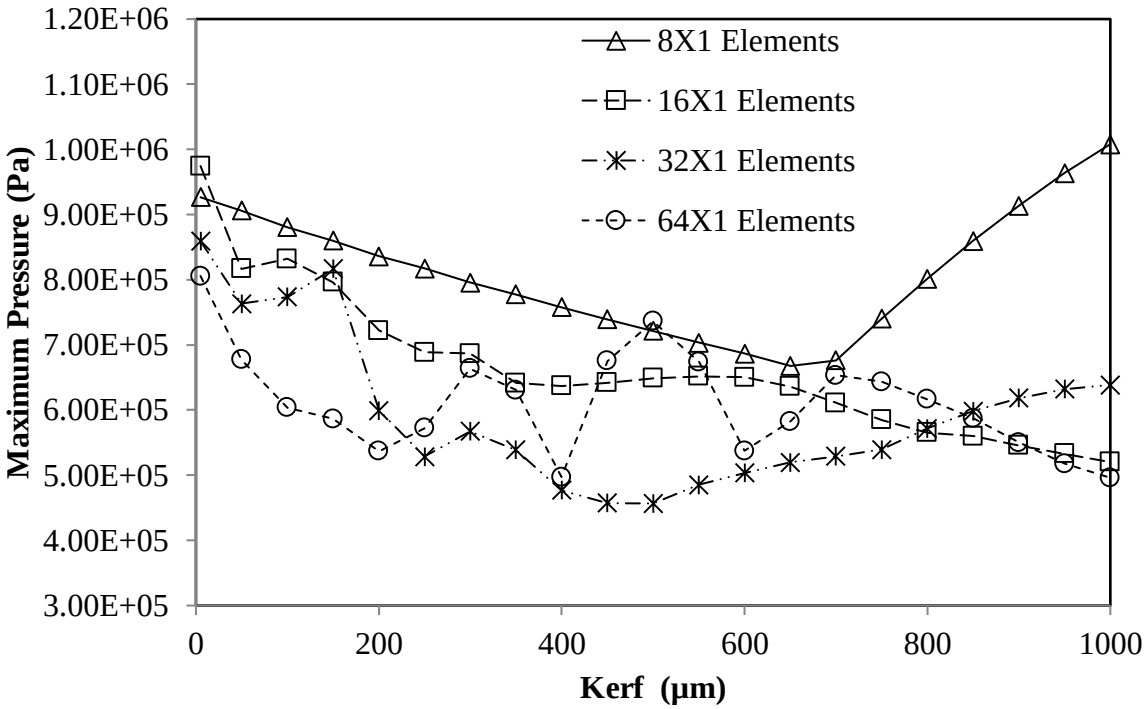

Figure 4.8 Changes in maximum pressure in simulated field within a kerf range of 5 µm to 1000 µm, for 8, 16, 32 and 64 x-elements (each element area = 4 mm × 0.5 mm) of cylindrical arrays focusing at 3.75cm distance. Here, each element's aspect ratio (height/width) is 1:8.

Figures 4.6 to 4.8 show the maximum pressure variations for different array arrangement forming a cylindrical shaped array. In this study, we have observed maximum pressure variation pattern with kerf. However, for getting optimum combination through evolutionary search method, we have used a constant kerf of 5 µm. Since a variable kerf will affect other design parameters in a fixed transducer area, such as, X and Y directional element numbers and height-width of each element.

4.2.2 Changes of Pressure Field with Width and Element Numbers

Element's width is another transducer array design variable that influences pressure field. When the width of transducer element changes while all other variables remain constant,

the total area of the transducer surface and height-width ratio also changes. For a rectangular transducer array, element's width ranging 0.3 mm to 2 mm, fluctuations of maximum pressures are shown in Figure 4.9.

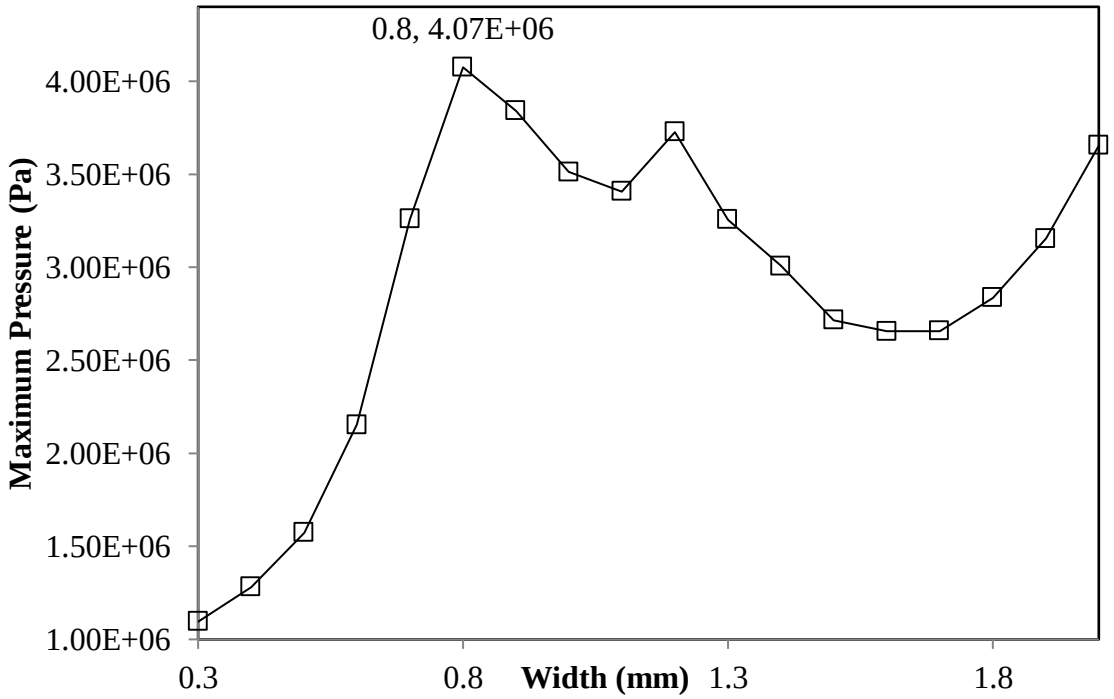

Figure 4.9 Changes in maximum pressure in simulated pressure field with variable width. Here, 20 by 1 rectangular array elements are focusing at 3.75 cm distance and height or kerf of each element are kept constant (height = 3 mm, kerf = 5 mm).

In a transducer array, typically narrow piezoelectric element width (typically between one-half to one wavelength) produces a diverging beam at a distance very close to the transducer face (Mahesh 2013). Figure 4.9 shows that, fluctuation of maximum pressure at focus zone varies with element width.

4.3 Genetic Algorithm (GA) Based Optimization

There are reports in the literature demonstrating the improvement of acoustic focusing ability of transducer by using optimized matching or backing layers geometry and by

using improved piezoelectric materials (Christoffersen, Wong et al. 2016). The pressure field optimization can also be done by changing the curvature of transducer surface. The results shown in Figures 4.3 to Figure 4.9 demonstrate that, design parameters, such as kerf, element's aspect ratio and shape of a transducer, all effect the pressure field at the focus zone. The influence of those parameters is coupled and complicated. In order to obtain the maximum pressure in the focus zone, those design parameters must be considered together. It is a challenge to find out an optimal or near optimal design shape and array distribution, because the formulas used to evaluate the pressure field is complex and highly nonlinear. Therefore, conventional optimization techniques are not suitable for this type of scenario.

To find an optimum arrangement of elements in this large volume of possibilities, Genetic Algorithm (GA) based evolutionary search is used in this study. A review of current literature shows that genetic algorithm has grown in popularity to solve optimization problems in diverse scientific research subjects for global robust search of an optimal value (Shim and Kim 2014). It also works fine with non-linear and high dimensionality functions. Recent studies also suggest that Genetic Algorithm have been applied with success in many complex design optimization problems (Rangel-Merino, López-Bonilla et al. 2005, Madani, Khanmohammadi et al. 2016). In this study, we explored the use of evolutionary algorithm for transducer shape and array arrangement optimization.

4.3.1 Selection of Design Variable and Their Ranges

The optimization process is done for several fixed transducer surface areas, ranging from 1 cm^2 to 16 cm^2. For each specified surface area, evolutionary based search is conducted

by varying the number of elements in two directions of the arrays. X-directional element range is set from 1 to 80 and Y-directional element range is set from 1 to 40. A constant 5 μm kerf is used for all sets of transducer surface areas. The pressure field of each combination of the parameters is evaluated by calling the function evaluation in the FOCUS package for ultrasound simulation. Numerical values of the maximum pressures in the simulated pressure field are then competed in a Genetic Algorithm based evolutionary search through MATLAB programming.

4.4 Element Numbers by GA

In our program, we have used a maximum number of 1000 iterations to find out optimum focus point and the stopping criteria is selected such a way that, if successive 10 iterations no longer produce better results, the simulation stops. The optimum numbers of X and Y elements in a 2D transducer array were determined for different surface areas. Figure 4.10 shows X directional element number search by GA programming for 2.64 cm^2 transducer surface area. For this area, the optimum X and Y element numbers found to be 21 and 10. Which means a total 210 elements with a single element area of 0.1184 mm^2 (1.5428 mm height and 0.07675 mm width) can be considered as an optimum shape. In this case, Rayleigh-Sommerfeld function evaluation was done 659 times and for optimization process total numbers of iterations in MATLAB were 993. Corresponding array distribution and the resultant pressure field generated by this 21 × 10 rectangular arrays are shown in Figure 4.11 (a & b).

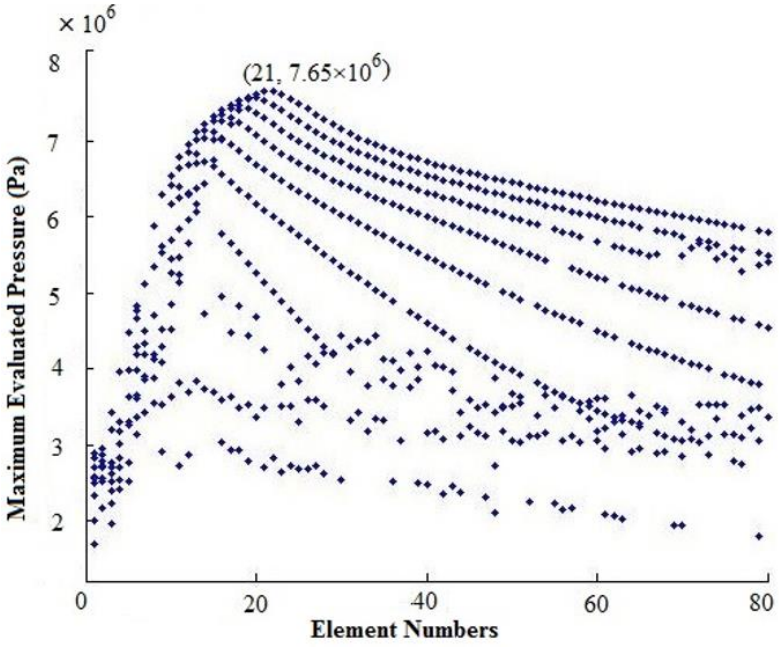

Figure 4.10 All evaluation values of Maximum pressure over X directional element numbers for a transducer surface area of 2.64 cm^2.

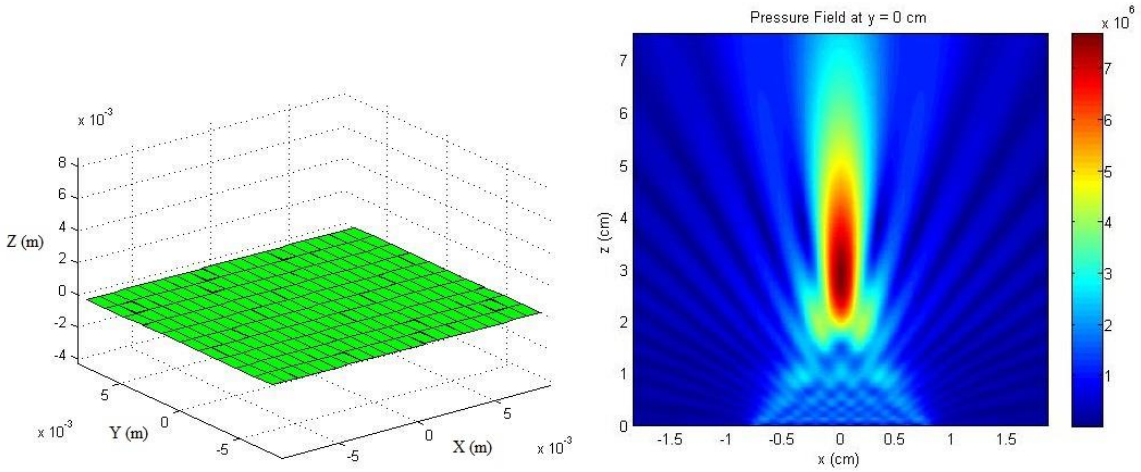

(a) (b)

Figure 4.11 (a) 21 × 10 array elements are arranged in 2.64 cm^2 surface with a kerf of 5 µm. (b) Simulated pressure field for 21 × 10 elements arranged in 2.64 cm^2 surface area focusing at 3.75 cm inside water media. Here, the maximum pressure found to be 7.65 MPa.

Figure 4.12 presents the total number of iterations and function evaluations done for each of the selected areas. In between 1 cm^2 to 16 cm^2, we have studied 25 different transducer areas for finding optimum X and Y directional element numbers and dimensions by using evolutionary search.

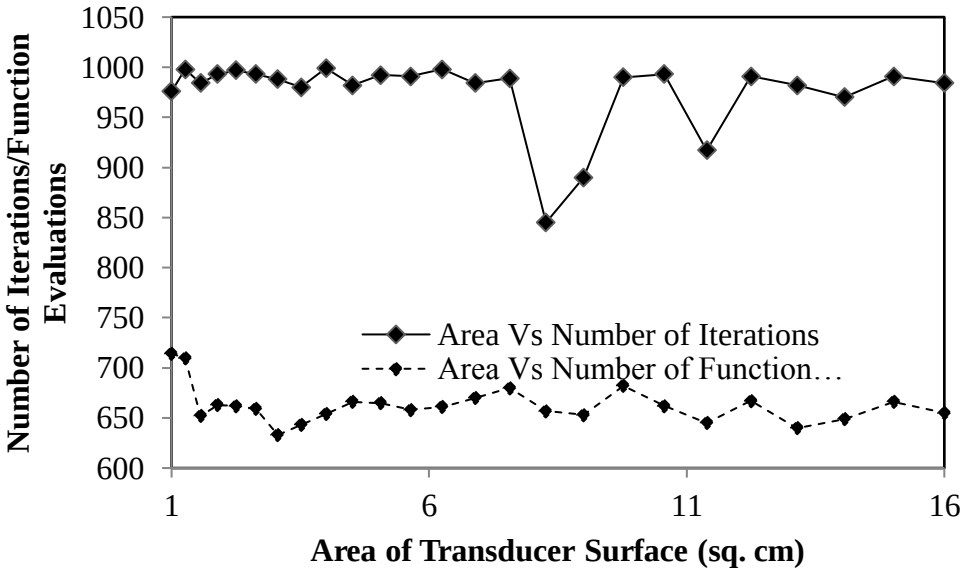

Figure 4.12 Number of function evaluations and number of iterations done for GA optimization process for different areas.

4.5 Optimization Results

The array element optimizations are tested for a range of transducer surface areas. As the total area increases the area of each element also increases, although their width-height ratio does not change in the same way. Figure 4.13 shows that, with the increasing transducer surface area the optimum maximum pressure tends to increase proportionally. However, by changing element numbers and arrangement, it is also possible to generate lower pressure for the same area.

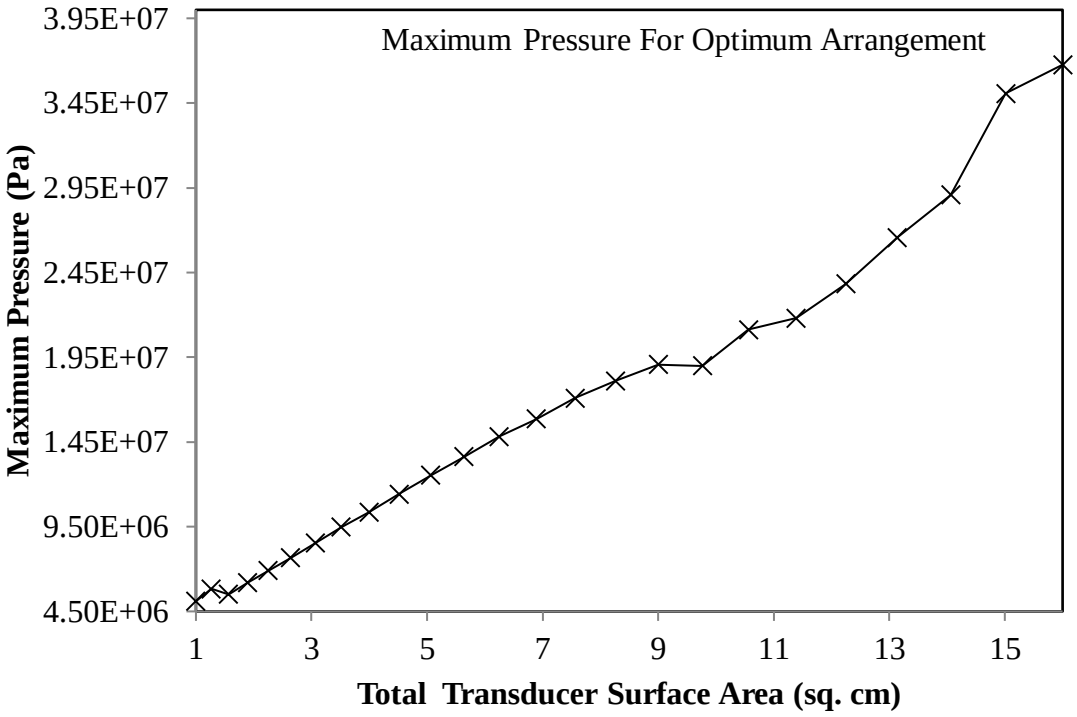

Figure 4.13 Maximum pressure found for optimum arrangements increases gradually with the total surface area.

Optimum element numbers are searched for areas ranging from 1 cm^2 to 16 cm^2 for similar width-height ratio of total transducer surface. As we increase the surface area, element numbers in X and Y direction changes gradually. Changes in optimum element numbers have been shown in Figure 4.14 for different transducer surface areas. Although we have set X-directional element range from 1 to 80, we have changed this limit to 1 to 120 for certain areas, where optimum element number reached to the boundary value 80.

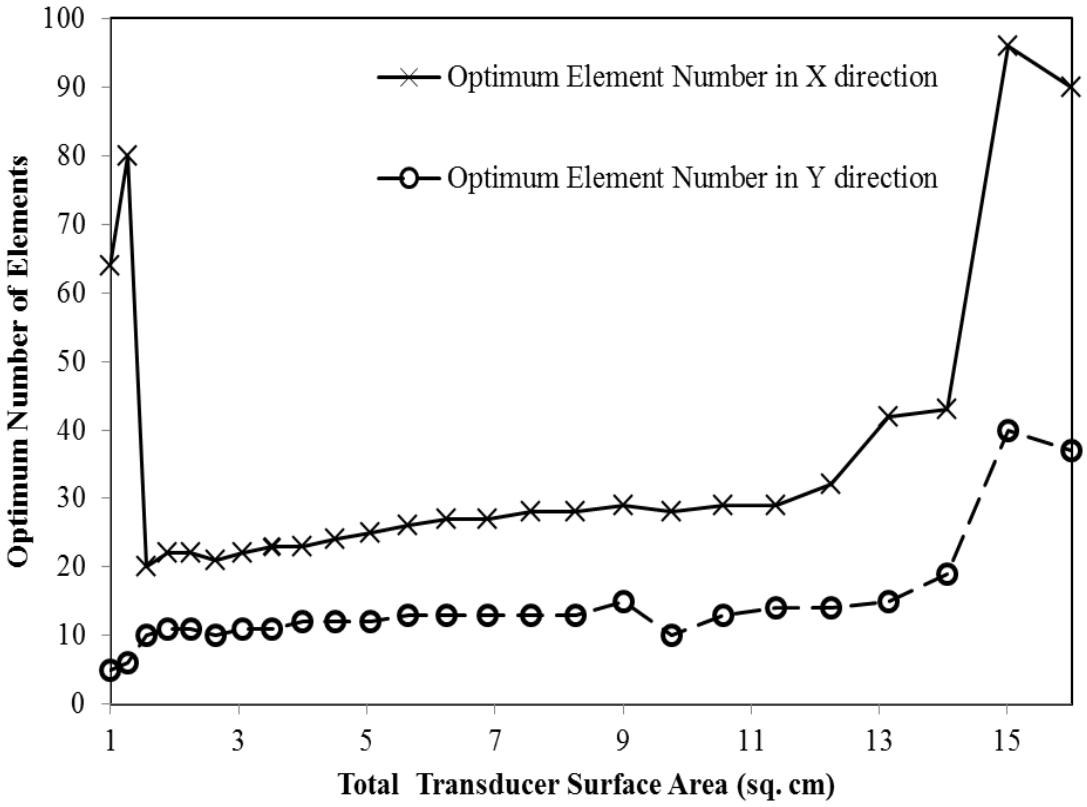

Figure 4.14 Changes in optimum element numbers in X and Y direction for different transducer surface area.

In a given amount of space, to achieve maximum pressures, required optimum element' number, dimensions and arrangements for 2D rectangular array are found for a range of areas. The results presented in this chapter for Genetic Algorithm based optimization covers only a range of transducer surface area (1 cm^2 to 16 cm^2) and element numbers (1 to 120), as the function evaluation time for each design arrangement is considerably large. According to our investigation, the pressure field is highly influenced by the transducer element's number and arrangements. Designs of ultrasonic surgical tools have many constraints to achieve accessibility over different parts of patient's body location. Therefore, if higher pressure can be generated by changing geometric arrangements of elements, transducers with required range of power can be

manufactured by investigating array distribution in the available design area. Although there are restrictions in creating array from manufacturing point of view, we assume that evolutionary based array element search method will open up opportunities for creating novel designs in future.

CHAPTER 5

FAST ESTIMATION MODEL FOR HOMOGENEOUS MEDIUM

5.1 Approach

Existing simulation models require considerable amount of time to complete one session of simulation. To select acoustic power and sonication time when planning treatments, many sessions of simulation may be needed. Previous simulation results contain huge amount of useful information and should be explored to guide and reduce the sets of simulations. This chapter introduces a methodology for making initial predictions for a single (homogeneous) medium based on patterns established with existing simulation results. The prediction model is not intended as replacement for accurate numerical simulations but instead for providing quick estimation of the effects of different sets of treatment parameters. This way, the number of the time-consuming simulations can be focused on a few sets of options. This study presents the methodology for developing such prediction models.

Set of maximum pressure and temperature values are obtained through simulation for various groups of tissue parameters by setting focus depth at 1 mm increment. Numerical values of maximum pressure field generated by using Rayleigh-Sommerfeld integral are plotted with respect to focus depth, ranging from 15 mm to 75 mm. Simulation parameters used for different tissue media are shown in Table 5.1.

Table 5.1 Simulation Parameters for Different Tissue Media (Duck 1990, Eikelder et al. 2016, Ginter 2000, Goss et al. 1980, Gowrishankar et al. 2004, Hand et al. 1982, Jungsoon et al. 2015, Rossetto, Diederich and Stauffer 2000)

Parameters	Unit[a]	Muscle	Liver	Water	Skin	Fat
Specific heat of blood	J/kg-K	3480	3480	3480	3480	3480
Blood perfusion	kg/m^3-s	2.3	15	0	5	0.54
Density	kg/m^3	1065	1050	1000	1200	950
Speed of sound	m/s	1575	1540	1500	1560	1478
Power law exponent	Unitless	1	1	1	2	1.4
Attenuation Coefficient	dB/cm-MHz	0.575	0.39	0.0025	2.5	0.61
Specific heat of the medium	J/Kg-K	3430	3639	4180	3400	3800
Thermal conductivity	W/m-K	0.4975	0.512	0.615	0.23	0.217
Nonlinearity parameter	Unitless	4.2	3.9	0	4.435	5.5

[a]Units are the same as International System Units(SI); J = Joule, kg = kilogram, K = kelvin, m = meter, s = second, dB = decibel, cm = centimeter, MHz = megahertz, W = watt .

Based on the plotted maximum pressure vs. focus depth patterns, mathematical expressions are obtained through a Gauss fitting model and only the rectangular element types of transducer geometries are used in the simulations to illustrate the methodology developed for constructing the prediction model. The same methodology can easily be extended to establish prediction models for other transducer design and medium parameters. The outline of this proposed fast estimation model is shown in Figure 5.1.

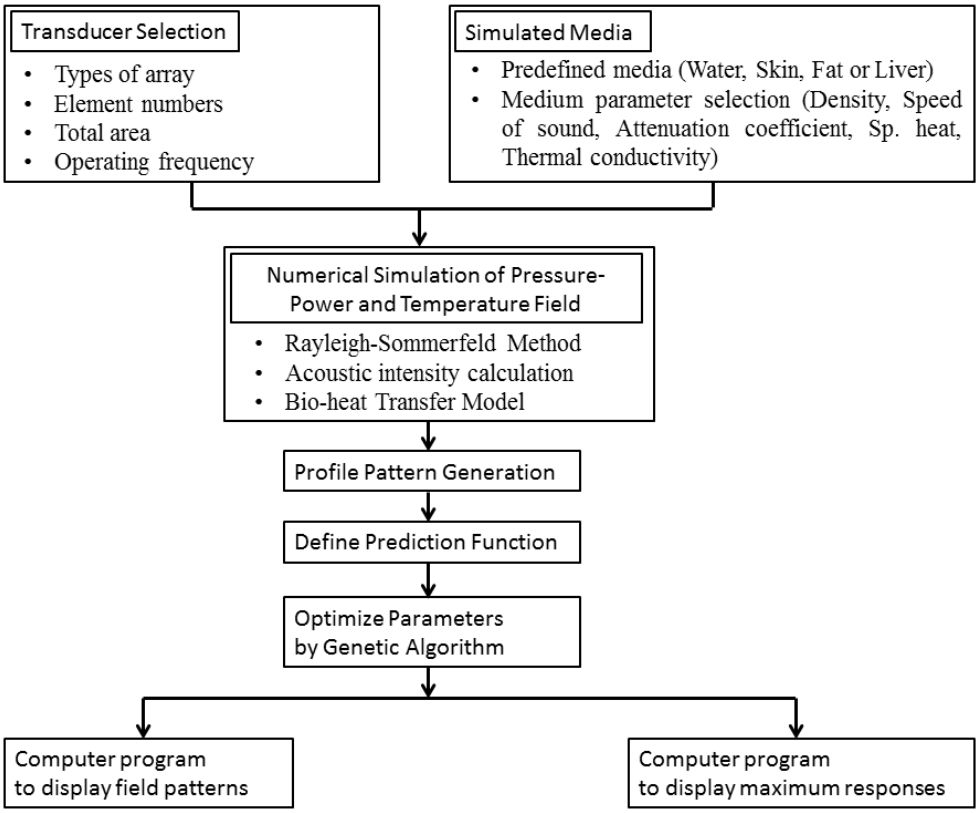

Figure 5.1 Outline of the development of fast estimation model.

5.2 Relation Between Pressure Field and Focus Distance

The pressure field pattern variation and maximum pressure generated at the focus zone have been obtained for a range of focus distance. Figure 5.2 (a) shows how the maximum generated pressure varies for a 16 by 1 element transducer as the focus distance changes for three different tissue medium sound velocities. The other internal tissue properties are kept similar as water media. Figure 5.2 (b) shows the effect of another internal tissue property (e.g., density) with maximum pressure. Here, three different fluctuation curves follow a similar pattern and these patterns depend on the transducer geometry and focus distance ratio. As internal tissue properties changes, the magnitude of pressure field sifted to a higher or lower value.

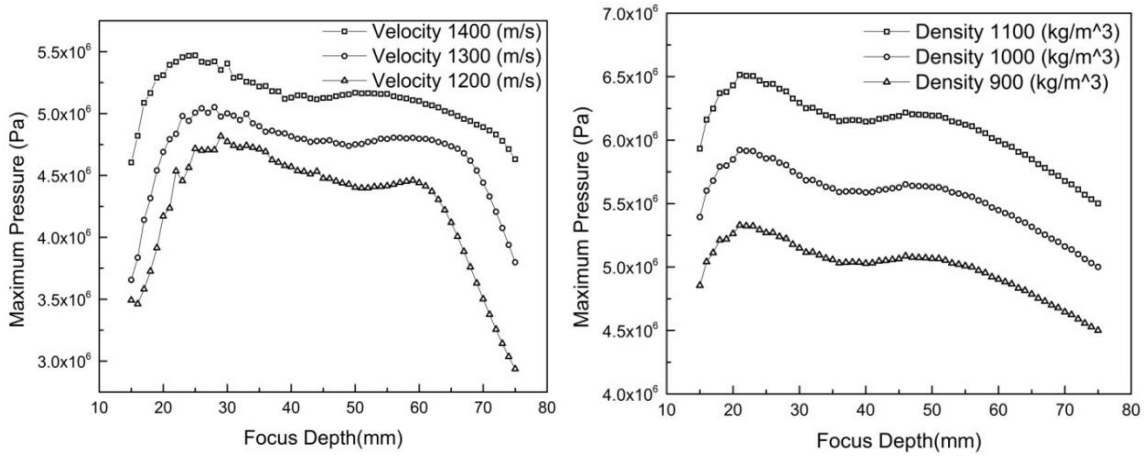

(a) (b)

Figure 5.2 Maximum pressure generated at different focus distance from a 16 by 1 phase array transducer (a) for three different sound velocities and (b) for three different densities of tissue media. Total transducer surface is 5cm by 1 cm, kerf 100 microns, and each element's height and width are 1 mm and 3.031 mm, respectively.

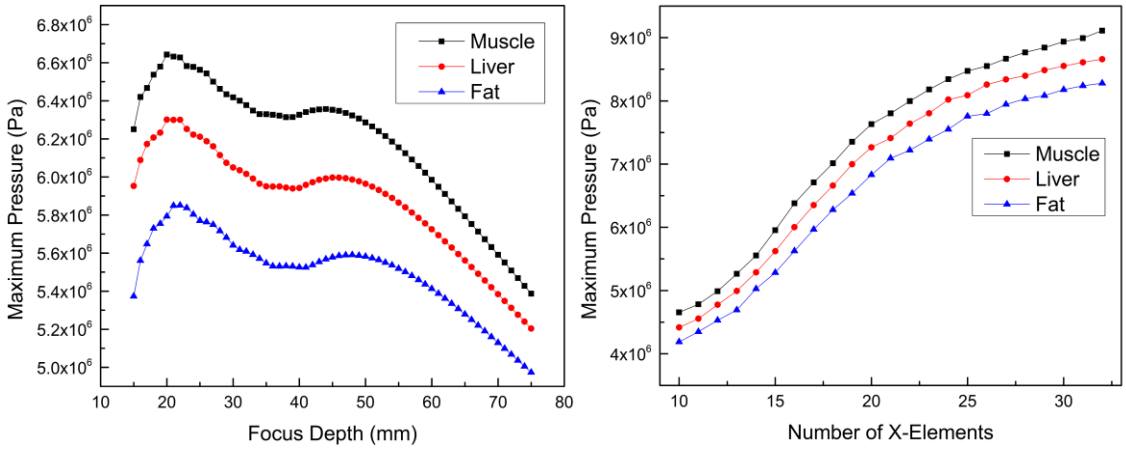

(a) (b)

Figure 5.3 (a) Maximum pressure generated at different focus distance from a 16 by 1 phased array transducer. Here, different tissue media were used to observe the effect of individual tissue properties on the output maximum pressure. Total transducer surface is 5 cm by 1 cm, kerf 100 microns, and each element height and width are 1 mm and 3.031 mm, respectively. (b) Increase in maximum pressure as we increase the element number on the transducer surface. Here, total transducer surface is 5 cm by 1 cm and element number varies from 10 to 35.

In Chapter 4 it has been shown that, pressure field pattern variation follows a fluctuation curve that may be determined by transducer's element arrangement, and by the ratio of transducer's area to focus distance. When specific media such as muscle, liver, water or skin are used in numerical calculations similar profile patterns can be obtained. Figure 5.3 (a) shows the variation of maximum pressure with respect to different focus depth for muscle, liver and fat media, and Figure 5.3 (b) demonstrates how these value increases at each point as we increase the source element numbers at the transducer surface.

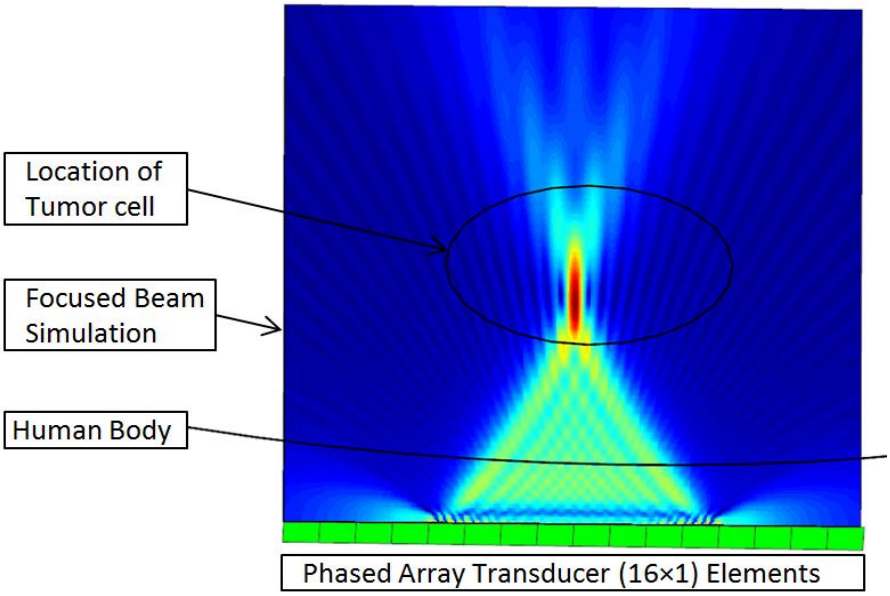

(a)

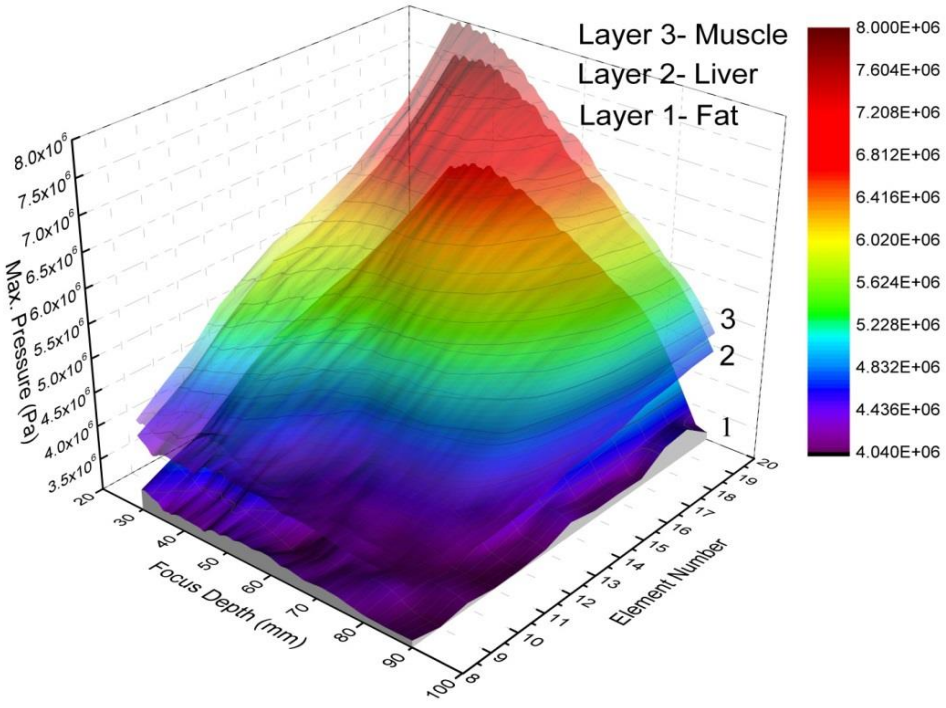

(b)

Figure 5.4 (a) A phased array Rayleigh-Sommerfeld focus simulation at a single point, by a transducer with 5 cm × 1 cm area and 16 × 1 array elements separated by 100 microns (kerf), focusing inside a fat tissue. (b) A partial representation of Figure 5.3 (a & b) where all maximum pressure field value at different focus depth (30 mm to 90 mm) for different transducer geometry (X-Element Number 8 to 20) are captured in 3D space.

5.3 Prediction Function

A fluctuation profile line fitting equation that can efficiently capture pressure field output variations at different focus depth with minimal error is defined. We used a Gaussian model function for defining multiple peaks and then the function parameters are optimized by using a Genetic Algorithm (GA) program. The Gaussian component parameters for different tissue media that are optimized are offset (y_0), center (x_c), width (w) and area (*A*). A Matlab program is developed to pick up the appropriate fluctuation profile component based on the transducer geometry and focus distance. The profile within our investigation limit (15 mm to 75 mm) is divided into two ranges based on the number of peaks and the overlapping peaks of the fitting curve are deconvoluted to find out combined Gaussian function by a peak decomposition program. Equation (5.1) represents the final model function used in current methodology and Figure 5.5 shows a fluctuation profile for 16 by 1 transducer element, with two Gaussian peaks.

$$y(x) = y_0 + \sum_{i=1}^{n} \frac{A}{w\sqrt{\pi/2}} e^{-2\frac{(x-x_c)^2}{w^2}} \tag{5.1}$$

Here, n = number of peaks of the selected fitting curve.

The Gauss function used to define a peak can be described by using four parameters: a center point (x_c), a variance (σ) equal to the half-width ($w/2$) of a peak, area under the curve (A) and the height of the peak. To define a curve with multiple peaks, a combination of multiple Gaussian function is used.

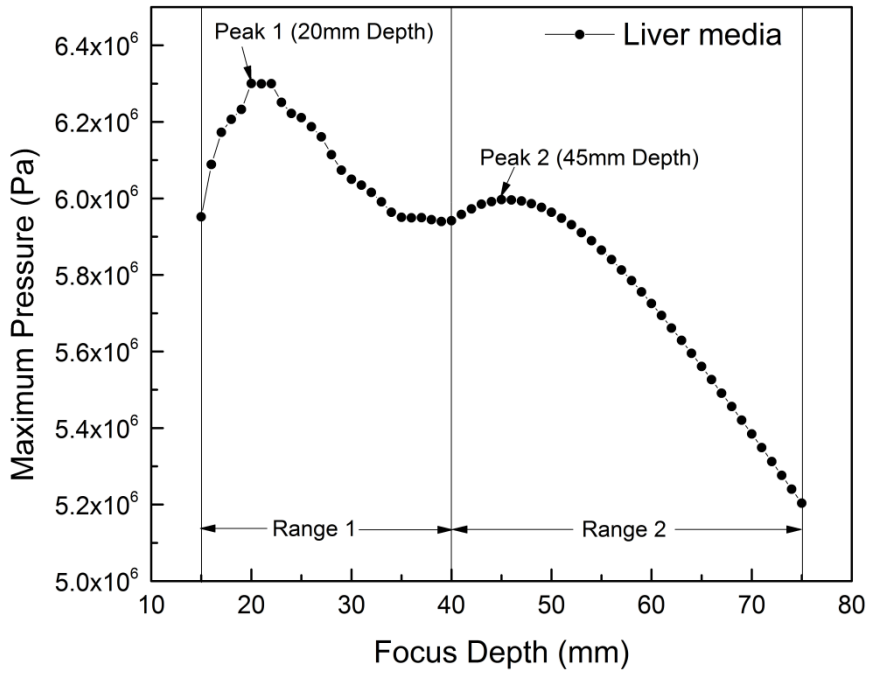

Figure 5.5 Fluctuation profile curve selected for a 16 by 1 array element is divided into two ranges.

A Matlab program is developed to pick up the appropriate fluctuation profile based on the transducer geometry and focus distance. Figure 5.5 shows a fluctuation profile for 16 by 1 transducer element, which is divided into two different ranges to define two Gaussian peaks. To optimize the prediction function profile fitting, a GA program is utilized for defining chromosomes for each parameter. The parameters (y_0, x_c, w, A) while represented by binary digits, are used to define the fitness of an organism and successive evaluated members are generated through crossover and mutation operators. The crossover operator randomly chooses a locus and exchanges between two chromosomes to create two offspring and then mutation operator randomly flips some of the bits in a chromosome. A pictorial representation of the GA crossover operators creating next generation of parameters is shown in Figure 5.6.

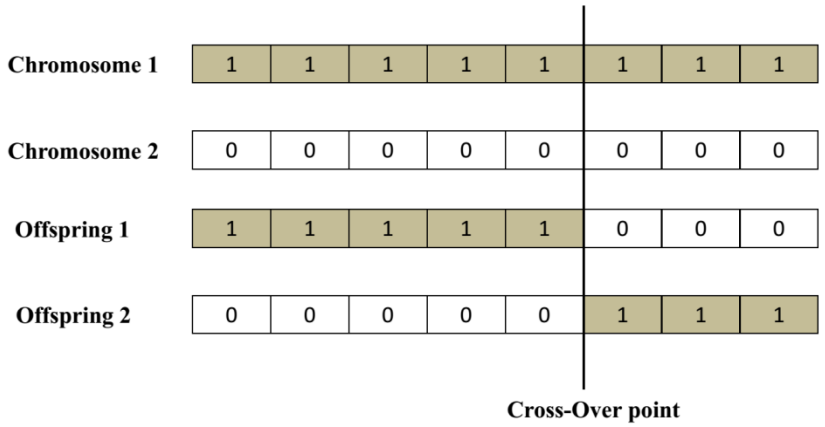

Figure 5.6 Pictorial representation of GA crossover operator exchanging bits of two binary chromosomes.

Once having the binary genetic code, the fitness function has been evaluated and only elite offspring with higher fitness value are allowed to compete in the next generation. The fitness function, which is defined by Equation (5.2), measures accumulated squared error with reference to Rayleigh-Sommerfeld simulation data.

$$F(y_0, x_c, w, A) = 1/SSE = 1/\sum_{j=1}^{n}[y_j - y(\mathrm{x})]^2 \qquad (5.2)$$

Here, $SSE = \sum_{j=1}^{n}[Maximum\,\mathrm{Pr}essure - \mathrm{Pr}ediction\,\mathrm{Pr}essure]^2$

In Equation (5.2), *SSE* is the Sum of Squared Error and *n* is the number of data points from actual numerical simulation. Higher fitness value of '*F*' will pass on to the next generation of evolution until the best set of fitness parameters are found. Figure 5.7 (a) shows example of curve fitting profiles before optimizing the Gaussian parameters. The blue curve is the resultant deconvolution profile for liver media before optimization

that is obtained through a computer program. Figure 5.7 (b) shows the fitted profile curve after the parameters are optimized through GA.

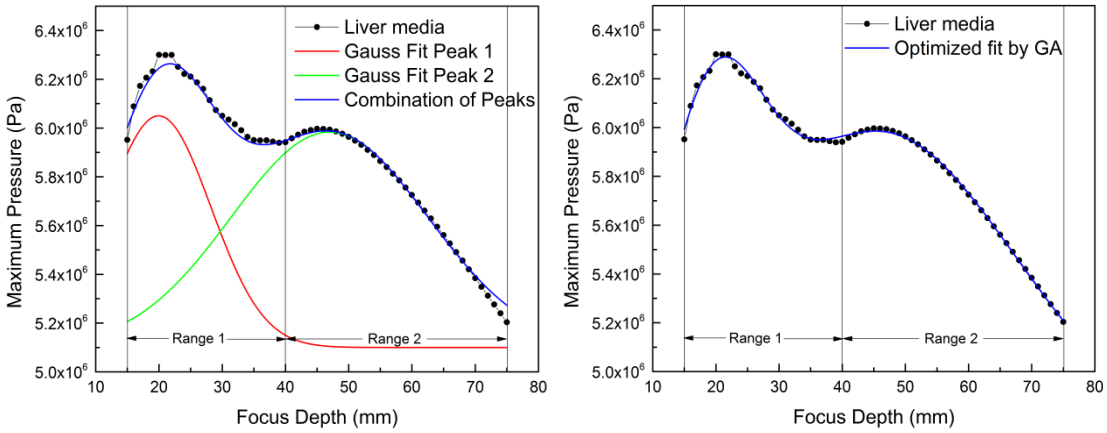

Figure 5.7 (a) Combination of Gaussian fitting profile of maximum pressure fluctuation curve for two different peaks in a liver medium. (b) Gaussian fitting profile curve for maximum pressure estimation in focus zone, obtained through Genetic Algorithm (GA) optimization.

5.4 Maximum Power and Temperature Profile Models

From the pressure field obtained by Rayleigh-Sommerfeld simulation, acoustic intensity can be calculated by using Equation (5.3). The acoustic intensity, I_A (W/m^2) is interpreted as the time-averaged rate of energy transmission of a sound wave through a unit area normal to the direction of propagation (Kinsler 2000).

$$I_A = \frac{1}{T}\int_0^T pudt = \pm\frac{P^2}{2\rho_0 c} \tag{5.3}$$

Here, T is one period of monochromatic wave; p is the instantaneous pressure, u is the particle velocity, P is the amplitude of plane wave, ρ_0 is the density and c is the speed of sound. Since power deposition is proportional to pressure distribution, the fluctuation curve for power deposition follow the same pattern as that of pressure field

distribution. Figure 5.8 (a & b) shows the fitting profiles for maximum output power deposition at focus zone before and after optimization through GA.

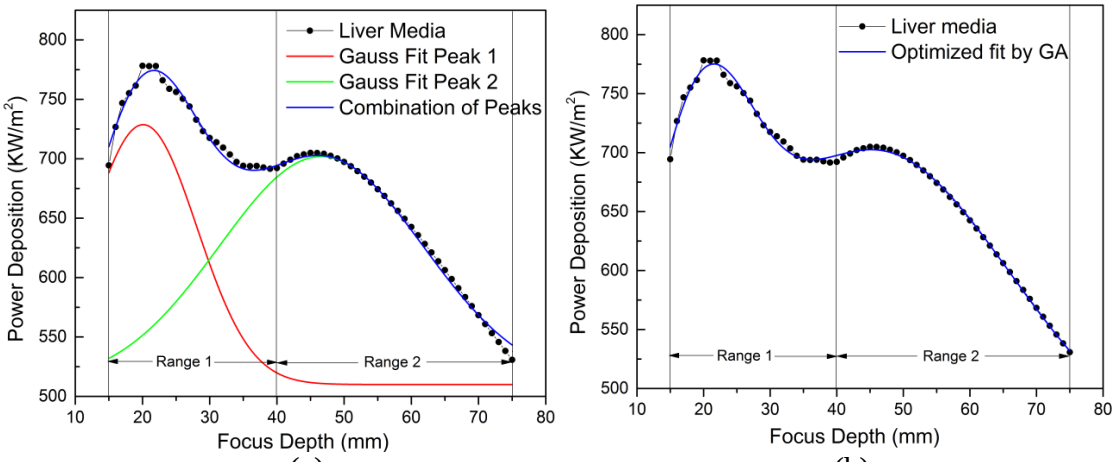

Figure 5.8 (a) Combination of Gaussian fitting profile of maximum power deposition fluctuation curve for two different peaks in a liver medium. (b) Gaussian fitting profile curve for maximum power estimation in focus zone, obtained through Genetic Algorithm (GA) optimization.

From the simulated 3D power deposition field, the steady state local temperature rise at each point is calculated by using Penne's bio-heat transfer model. For a steady state problem, it is given by the Equation (3.3) (Pennes 1948, Moros, Roemer et al. 1988). Equation (3.3) can be solved through an iterative finite difference scheme that discretizes the three-dimensional computational volume in a rectilinear grid (Ocheltree and Frizzell 1987, Zeng, Li et al. 2010). Using a central difference approximation of the second order derivative this equation can be expressed as,

$$K\left[\frac{T^{i+1,j,k}-2T^{i,j,k}+T^{i-1,j,k}}{\delta^2}+\frac{T^{i,j+1,k}-2T^{i,j,k}+T^{i,j-1,k}}{\delta^2}+\frac{T^{i,j,k+1}-2T^{i,j,k}+T^{i,j,k-1}}{\delta^2}\right] -W_bC_bT^{i,j,k}+Q^{i,j,k}=0 \quad (5.4)$$

In Equation (5.4), *i, j, k* represents the indices of the grid points in x, y and z directions, δ is the uniform step size between the grid points and $Q^{i,j,k}$ is the power deposition in that unit volume. The expression for calculating temperature at a grid point, $T^{i,j,k}$, can be found by rearranging Equation (5.4).

$$T^{i,j,k} = \frac{K}{6K + W_b C_b \delta^2}\left[\frac{\delta^2}{K} Q^{i,j,k} + T^{i+1,j,k} + T^{i-1,j,k} + T^{i,j+1,k} + T^{i,j-1,k} + T^{i,j,k+1} + T^{i,j,k-1}\right] \qquad (5.5)$$

Equation (5.5) gives the steady state temperature rise at each grid point corresponding to the power deposition rate and the solution of it converges after multiple iterations.

The local temperature rises obtained through bio-heat model do not follow the same pattern of pressure field distribution as the heat transfer in tissue depends on both conduction and convection mechanism. The bio-heat model used in numerical simulations assumes tissue volume as a continuum, having only micro-circulatory blood channels. Equation (3.2) accounts for conduction and convection losses due to heat dissipation and blood circulation. Here, the arterial bold temperature was set to 37°C and temperature rise profile is defined from 37°C by using two separated peaks without deconvolution. The temperature rise pattern with respect to power deposition along with the Gaussian fitting profile is shown in Figure 5.9 (a) and the Gaussian fitting profile curve after applying GA optimization is shown in Figure 5.9 (b).

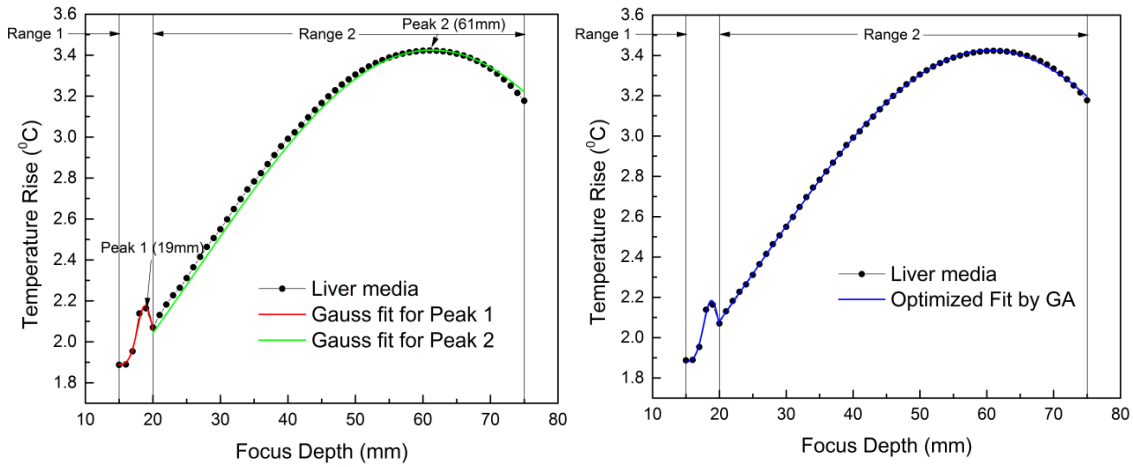

(a) (b)

Figure 5.9 Gaussian curve fitting of temperature rise profile in liver media (a) before optimizing the fitting parameters and (b) after optimizing the fitting parameters by using GA.

A set of optimized profile fitting parameters found for a 16 by 1 element transducer focusing inside liver media is presented in Table 5.2. Root Mean Squared Error (RMSE) of the fitting curve shown in this table, illustrates improved fitting condition by GA optimization. For a liver media, before applying genetic algorithm to the profile fitting curve, average Root Mean Squared (RMS) error of the model were 28 kPa for pressure, 5.2 kW/m^2 for power and 0.046°C for temperature rise. After getting optimized profile fitting by Genetic Algorithm, average RMS error were improved to 12.257 kPa for pressure, 2.99 kW/m^2 for power and 0.0261°C for temperature rise.

Table 5.2 Fitting Parameters of Prediction Function Before and After Applying GA Optimization for Liver Media

		Before Optimization		After Optimization	
Gauss Fitting Profile	Parameters	Peak 1	Peak 2	Peak 1	Peak 2
Pressure	y0	5.03E+06	-	4.70E+06	-
	xc	0.01962	0.04666	0.019105	0.0458
	w	0.01637	0.03445	0.01575	0.042951
	A	19541.71	39555.00	18876	69006
	RMSE[a] of combined profile	28058		12257	
Power Deposition	y0	457667.5417	-	4.40E+05	-
	xc	0.01949	0.04578	0.01941	0.045631
	w	0.01545	0.03915	0.015275	0.040613
	A	4185.58507	11638.11	4095	13340
	RMSE of combined profile	5215.7		2990.8	
Temperature Rise	y0	1.88741	0.701	1.87732	0.7005
	xc	0.01885	0.0613	0.01881	0.06048
	w	0.00229	0.069	0.00234	0.06943
	A	8.28E-04	0.236	9.00E-04	0.2371
	RMSE of combined profile	0.0464		0.0261	

[a]RMSE = Root Mean Square Error.

5.5 GUI Software for Prediction Model

A computer program with Graphical User Interface (GUI) has been developed for the prediction model. The prediction function Equation (5.1) is used to calculate the maximum pressure, power deposition and temperature rise at the focused zone. The

optimized profile fitting parameters for $y_0, x_c, w \; and \; A$ obtained through GA optimization have been stored in the program and these parameters are utilized to solve the model equation for variable focus depth 'x' inside different tissue medium. According to numerical simulations, the pressure, power and temperature field pattern is not affected by tissue medium or its internal properties (density, velocity, attenuation coefficient etc.), but their magnitude at each point shift to a different value in a similar fashion. Both Rayleigh-Sommerfeld and Angular Spectrum based output pattern mapping through parallel planes depends only on the transducer geometry and focused distance.

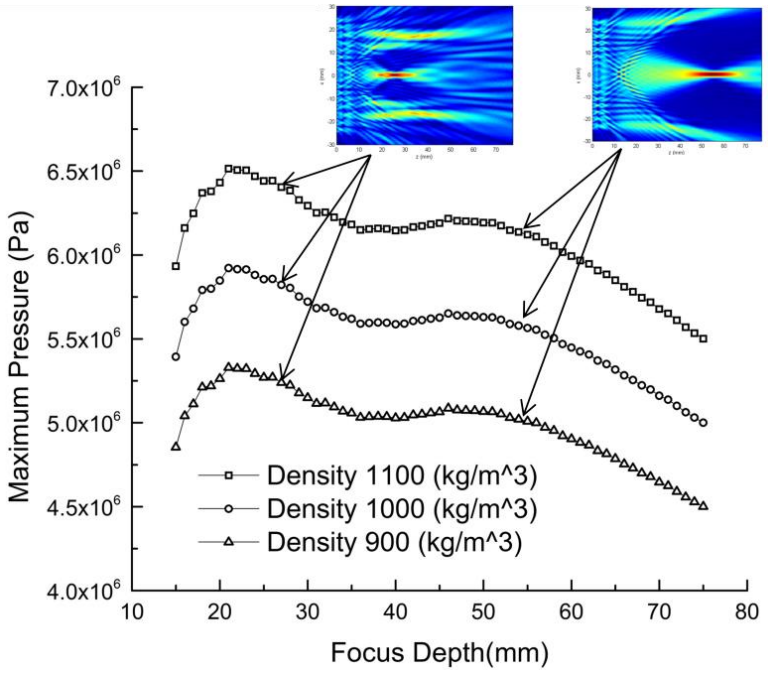

Figure 5.10 Output pressure field pattern obtained through Rayleigh-Sommerfeld model for 26 mm and 55 mm focus distance in different density tissue media.

Figure 5.10 shows that the output pressure field pattern by Rayleigh-Sommerfeld simulation remains similar for 26 mm and 55 mm focus distance in different density tissue media. In focused ultrasound simulations, this field pattern visualization is necessary to find out possible hot spot locations.

We implemented a pattern visualization method in GUI program along with the maximum response calculation through model function. In this method, a set of pressure, power and temperature field pattern obtained by Rayleigh-Sommerfeld calculation is stored within each 0.5 mm focus gap. When the GUI model calculates output pressure or temperature based on the prediction function, it also shows the field pattern of the nearest 0.5 mm distances. For example, in GUI sliding bar, if a focus depth of 44.45 mm is selected, the program will show patterns for 45.5 mm focus depth. Figure 5.11 shows the GUI program to represent the prediction model discussed in this study. The maximum pressure, power and temperature generated in the focused zone are calculated by using prediction functions. The slider bar in this interface is able to change the focus depth continuously. At the same time, maximum pressure, power and temperature rise at certain focus depth can be obtained by pressing respective push buttons that calculate the prediction function.

In Figure 5.11, the model shows that for a focus depth of 29.1401 mm the maximum pressure obtained is 6.07 MPa, power deposition is 723.22 kW/m^2 and temperature rise is 2.5133 °C at the focused zone. The pressure field, power field and temperature field shown in the GUI program can be updated dynamically with the movement of sliding bar.

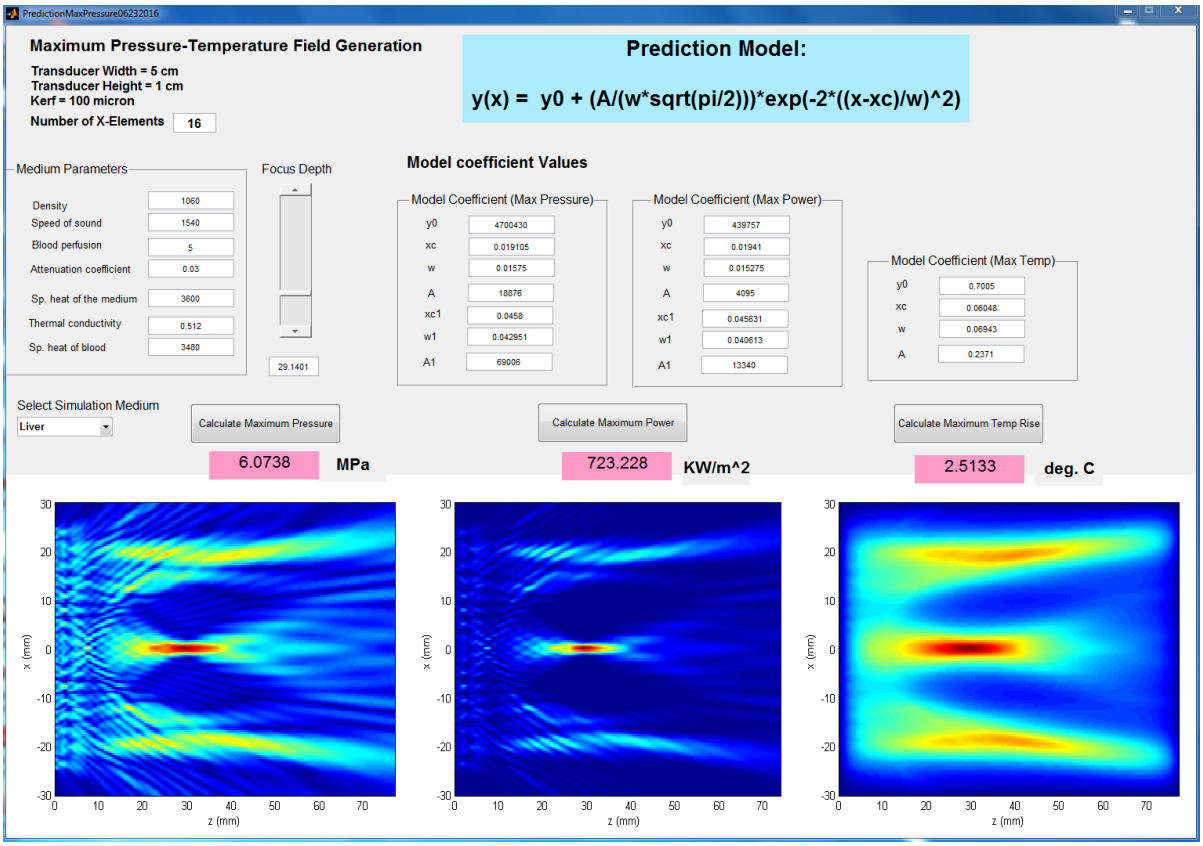

Figure 5.11 GUI program of estimation model to calculate maximum pressure, power deposition and temperature rise along with field pattern visualization.

5.6 Model Validation

Pressure variation patterns with respect to transducer geometry and focus depth are used to establish an estimation model that is able to provide maximum pressure and temperature values instantaneously with a good accuracy. In recent years, researchers developed many different computational algorithms to predict temperature and beam profile pattern. Some of these computations are very time consuming (~1 day) depending on the computation power and required accuracy. Other computations must go through several approximations to provide a faster estimation time. If many sets of simulations can be done in a short period of time, it would assist the initial design steps of transducers

and operation planning of focused ultrasound therapy. Since many of the HIFU devices are at the experimental stage, results obtained from computer simulations are highly beneficial for optimization of power deposition parameters. A fast simulation method would facilitate the process of optimization as well as transducer geometry selection. Fast simulation can also help surgeon to make quick decision and allow doing many trials on simulations.

Since speed of HIFU simulations has always been a very critical issue, there are several research studies that use various approximations with Rayleigh-Sommerfeld method to find fast output pressure-temperature field. A typical Rayleigh-sommerfeld calculation in homogeneous media takes 20 to 30 minutes and a typical Angular Spectrum calculation takes about 1 to 10 minutes to finish in a computer system with Intel(R) Core i7, Dual core 2.00 GHz processor and 16.0 GB memory (RAM). But these calculation times increase significantly with the complexity of tissue position. To validate the estimation model, it's results are compared to the results found from Rayleigh-Sommerfeld and Angular Spectrum method.

5.7 Results and Discussion

To check the performance of the model, five random data points were generated through a program within selected focus range (15 mm to 75 mm). HIFU beam is simulated in these focus distances for liver, fat and muscle tissue media. After the evaluation, the output Maximum pressure, power deposition and temperature rise at these five random points are compared with the Rayleigh-Sommerfeld and Angular Spectrum simulations.

Average model error found in the model for liver, fat and muscle media at respective points are shown in Table 5.3.

Table 5.3 Prediction Model Comparison with Rayleigh-Sommerfeld and Angular Spectrum Method at Random Data Points for Homogeneous Liver, Fat and Muscle Media

		Prediction Model			Rayleigh-Sommerfeld			Angular Spectrum		
	Focus Depth	Maximum Pressure	Power Deposition	Temp. Rise	Maximum Pressure	Power Deposition	Temp. Rise	Maximum Pressure	Power Deposition	Temp. Rise
Unit[a]	mm	MPa	KW/m^2	°C	MPa	KW/m^2	°C	MPa	KW/m^2	°C
	60.249	5.723	642.012	3.425	5.718	640.839	3.422	5.707	638.618	3.417
	47.837	5.978	700.503	3.250	5.988	702.900	3.274	6.003	706.430	3.273
Liver	48.209	5.975	699.907	3.260	5.985	702.145	3.262	6.006	707.282	3.282
tissue	35.125	5.954	694.760	2.787	5.950	694.011	2.788	6.021	710.831	2.839
	72.428	5.295	549.475	3.266	5.297	549.977	3.254	5.285	547.599	3.253
Average % Model Error					0.105	0.208	0.252	0.501	1.003	0.770
	53.056	5.548	5.120	0.0261	5.550	5.134	0.0261	5.587	5.203	0.0265
	51.027	5.568	5.156	0.0258	5.573	5.177	0.0257	5.628	5.278	0.0261
Fat	69.551	5.146	4.405	0.0262	5.143	4.409	0.0263	5.177	4.468	0.0266
tissue	49.250	5.578	5.176	0.0254	5.587	5.202	0.0253	5.634	5.290	0.0257
	52.834	5.550	5.124	0.0261	5.553	5.140	0.0261	5.588	5.204	0.0264
Average % Model Error					0.075	0.302	0.262	0.797	1.789	1.141
	72.127	5.505	1355.32	8.454	5.504	1357.313	8.470	5.528	1369.08	8.474
	41.395	6.348	1802.70	8.148	6.344	1803.493	8.145	6.368	1816.94	8.208
Muscle	51.092	6.265	1755.83	8.775	6.263	1757.318	8.789	6.289	1772.12	8.839
tissue	28.215	6.461	1867.08	6.717	6.452	1864.960	6.706	6.507	1896.89	6.789
	55.726	6.142	1687.80	8.909	6.133	1685.158	8.900	6.157	1698.47	8.942
Average % Model Error					0.080	0.109	0.128	0.412	0.981	0.625

[a]Units are the same as International System Units(SI); m = meter, mm = millimeter, MPa = mega pascal, KW = kilo watt, °C = degree centigrade.

For liver, fat and muscle tissue, average model error in pressure estimation compared to Rayleigh-Sommerfeld model are 0.105%, 0.075% and 0.08%, respectively and compared to Angular Spectrum method these errors are 0.501%, 0.797% and 0.412%, respectively. Average model error for maximum power deposition and temperature rise are also found to be minimal.

When the estimation model is integrated with GUI program, it can give almost instantaneous results at different focus distances selected through GUI sliding bar. The accuracy of the model depends on the profile fitting method used in this study. Although GA based evolutionary search can be a robust way to select optimum fitting parameters, the success of utilizing this method depends on the starting point of the search. We used a Matlab program to find the fitting parameter values initially and later these values are used as starting point of search in GA optimization to evaluate our objective function.

The results show that optimized prediction model can quickly and efficiently capture responses of focused ultrasound beam. This fast prediction method can also be extended for various tissue media and geometries by adding optimized parameter components to the model.

CHAPTER 6

FAST ESTIMATION MODEL FOR HETEROGENEOUS MEDIUM

6.1 Approach

Heterogeneous or layered tissue media presents more realistic scenario for HIFU surgery. But the time and computer memory required to do this simulation is relatively very expensive. Many times, HIFU operators assume a homogeneous medium for doing a quick simulation and for avoiding computational complexity. In this Chapter, heterogeneous tissue media with parallel layers that is found in average human body is considered to establish a fast estimation model. The general overview and steps of the prediction methodology is similar to that of homogeneous medium presented in Figure 5.1. An extended Rayleigh-Sommerfeld method was developed that can address beam refraction and reflection in multiple tissue layers.

6.2 Modified Simulation Method for Heterogeneous Media

In a heterogeneous media, tissue layers can change the wave pattern significantly due to the reflections and diffractions in the tissue boundaries. In this section, a method for calculating Rayleigh-Sommerfeld pressure field, that can handle transmission of acoustic waves in tissue layers is presented. A heterogeneous media consisting of four parallel tissue layers that is found in HIFU therapy for Kidney Pancreas and Viscera tissues, is considered for this simulation and the schematic of selected four tissue layer thicknesses is shown in Figure 6.1.

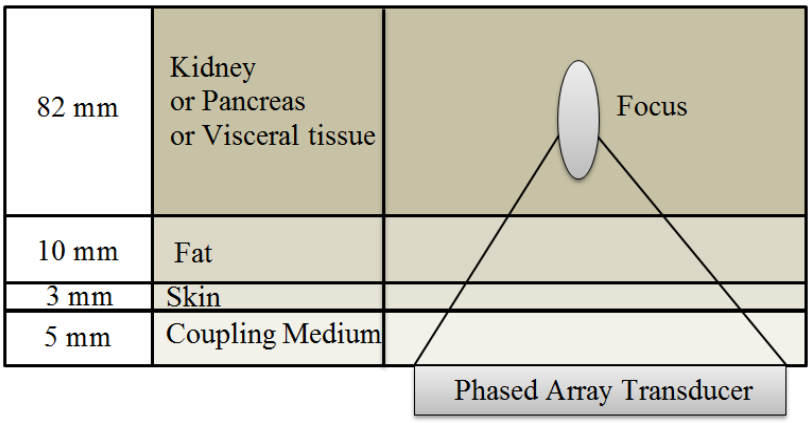

Figure 6.1 Heterogeneous tissue media with parallel layers for Rayleigh-Sommerfeld simulation.

To achieve the combined effects in layered media, Rayleigh-Sommerfeld model is applied first to obtain output pressure field in each grid volume separately. When ultrasound wave hits the interface between two media, some part of the wave is reflected in the first medium and other part is transmitted through the second medium. The pressure values at each coordinate grid volume are recalculated by multiplying those with respective transmission coefficient matrices (Kinsler 2000) and by using updated focus phases source plane. The updated simulation grid volumes for each tissue layer are then placed together to find the resultant time harmonic pressure field response. Transmission coefficient (T_p) matrix calculation is based on Snell's law and it is defined by Equation (6.1) (Christopher and Parker 1991, Clement and Hynynen 2003).

$$T_p = \frac{2}{1+\frac{\rho_1 c_1 \cos\theta_t}{\rho_2 c_2 \cos\theta_i}} \qquad (6.1)$$

Here, θ_i and θ_t are incident and refraction angles, $\rho_1 c_1$ and $\rho_2 c_2$ are acoustic impedances in first and second media respectively. A schematic of developing resultant pressure field in layered media is shown in Figure 6.2.

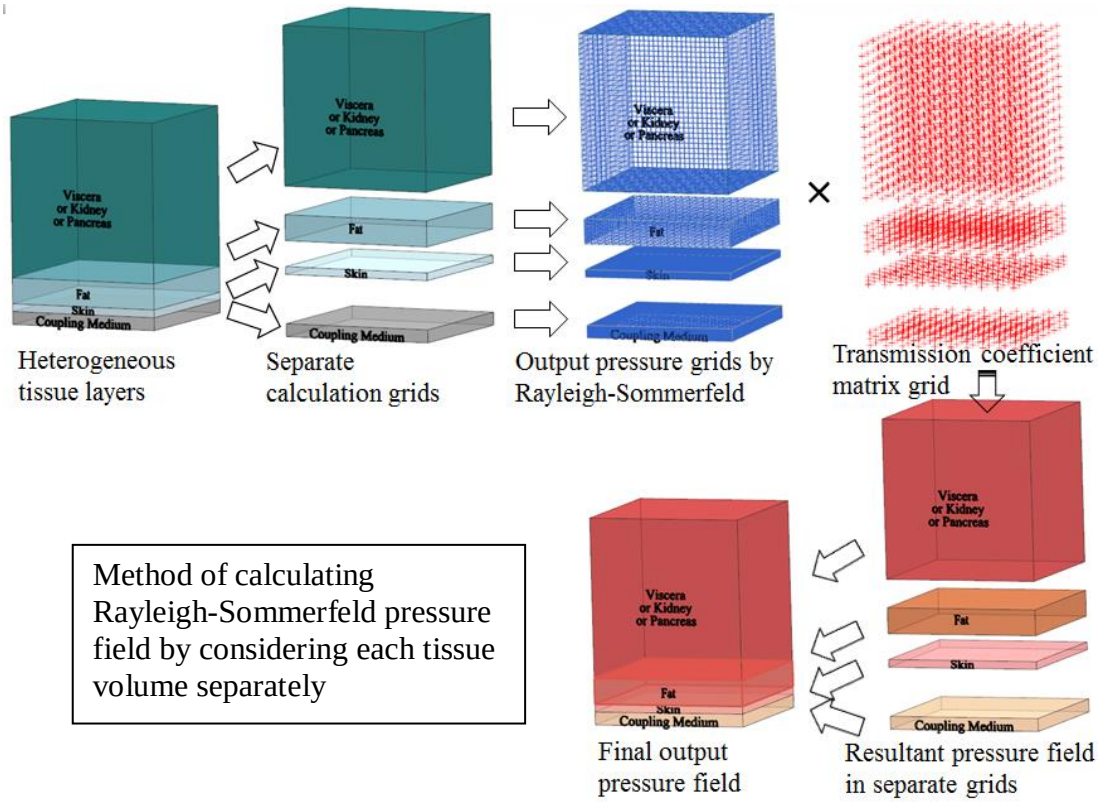

Figure 6.2 Schematic of pressure field calculation method for a heterogeneous media.

6.3 Validation of the Modified Simulation Method

MR-guided rectangular phased array transducer is clinically tested for the treatment of prostate hyperthermia treatment by several researchers. In this section, the modified Rayleigh-Sommerfeld simulation method is validated by comparing it's result with experimental data from literature, where a commercial MR-guided endo-rectal ultrasound phased array transducer (ExAblate 2100, Insightec, LTD.) is studied through 3D finite

element based bio-thermal computer simulation and *ex vivo* experiment (Salgaonkar, Prakash et al. 2013).

The ultrasound phased array transducer used in the experiment, has 990 elements, arranged linearly over 23 mm × 40 mm surface area. A picture of this transducer, ExAblate 2100, is shown in Figure 6.3. The transducer device of this system can be coupled with rectal wall through a latex balloon containing degassed water. Additionally, with the help of positioning and motion units it can focus ultrasound beam at different angles inside prostate.

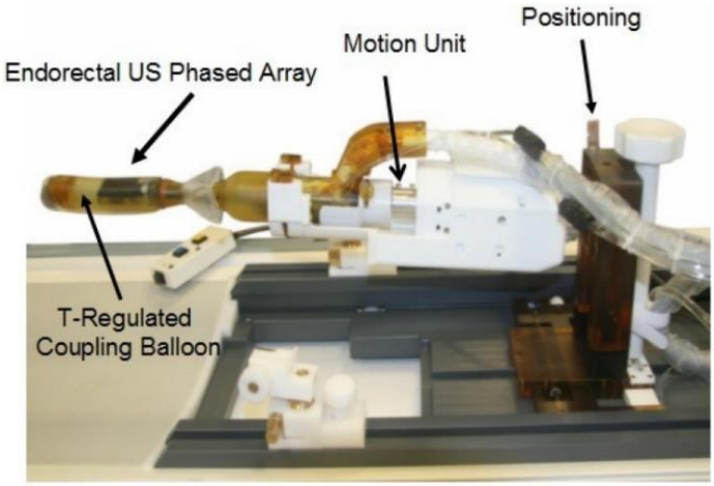

Figure 6.3 Photograph of ExAblate 2100 endo-rectal phased array prostate ablation system with positioning and motion units (Salgaonkar, Prakash et al. 2013).

In the experiment, along with MR-guided visualizing technology, a MR temperature monitoring system with 3.0T magnetic strength is used to check temperature rises. Similar boundary conditions and tissue properties as given in the experimental study are used in the modified Rayleigh-Sommerfeld method to obtain simulation result for comparison.

6.3.1 Experimental Procedure

In Salgaonkar, Prakash et al. 2013, tissue mimicking phantom materials for prostate and periprostate are used for the ex-vivo experiment. Ultrasound beam is focused using ExAblate 2100 phased array transducer and during the process, temperature rise profiles are monitored by using a 3.0T MRI scanner (GE Helthcare MR 750). A schematic of the temperature monitoring system using two 5-inch surface imaging coils and temperature rise profile are shown in Figure 6.4. The temperature rise is measured through MR thermometry and it is performed in real time using RTHawk (HeartVista Inc, Palo Alto, CA) software.

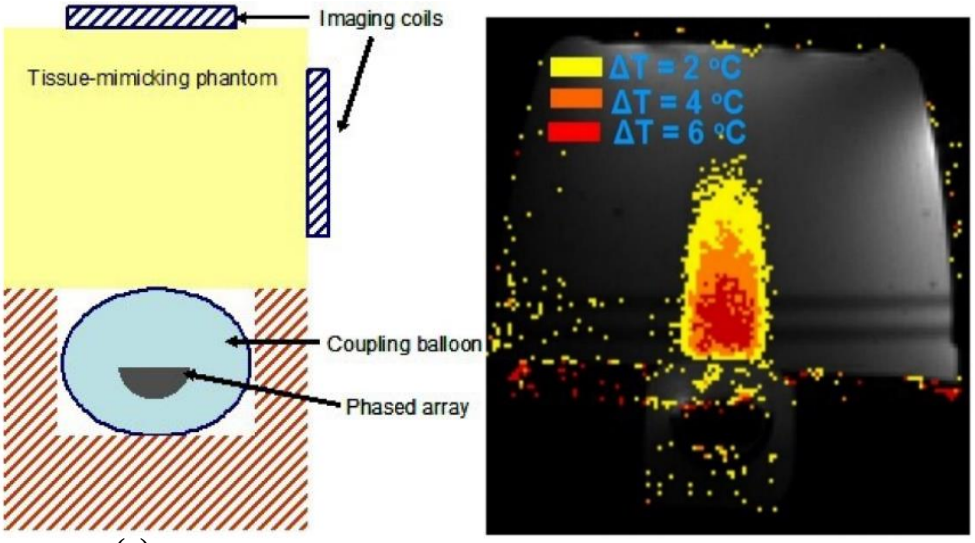

(a) (b)

Figure 6.4 (a) A schematic of the experimental setup by Salgaonkar, Prakash et al. 2013, (b) CW sonication in tissue mimicking phantoms with ExAblate 2100 array operating at 0.86 W/cm^2. The heating is done from electronically scanned sonication using three multiplexed focal positions at 40 mm depth and 5 mm, 0, -5 mm azimuth (Salgaonkar, Prakash et al. 2013).

6.3.2 Heterogeneous Rayleigh-Sommerfeld Method

The heterogeneous media is constructed using four parallel tissue layers. ExAblate 2100 transducer is operated from a coupling balloon filled with degassed water and after that

layers of rectum wall, periprostate and prostate tissues are used. Tissue properties used in our simulation are selected from Finite Element Method (FEM) studies by Salgaonkar, Prakash et al. 2014. Figure 6.5 shows the schematic of tissue layers used in simulation.

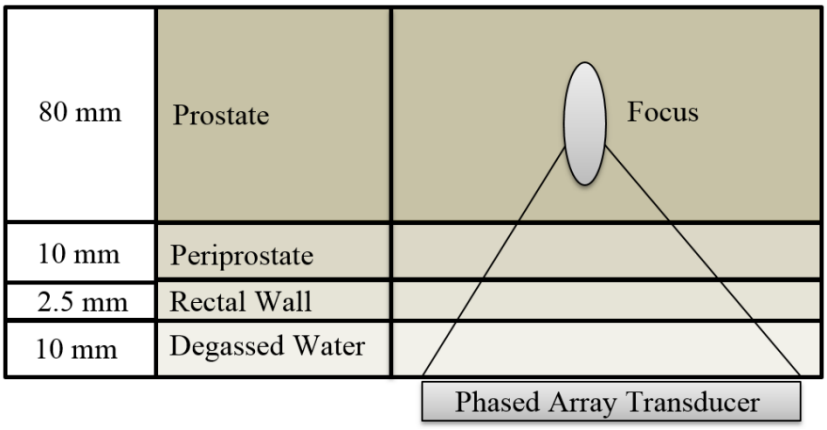

Figure 6.5 Schematic of tissue layers for modified Rayleigh-Sommerfeld simulation.

The maximum temperature rise found by modified Rayleigh-Sommerfeld method is 7.2°C, which is about 1°C higher than the rise reported in the experimental study. A little high temperature is valid, as in simulation degassed water was not regulated for transducer cooling and tissue wall protections. Figure 6.6 shows the temperature profile pattern in our simulation which seems to be consistent with MR temperature profile images.

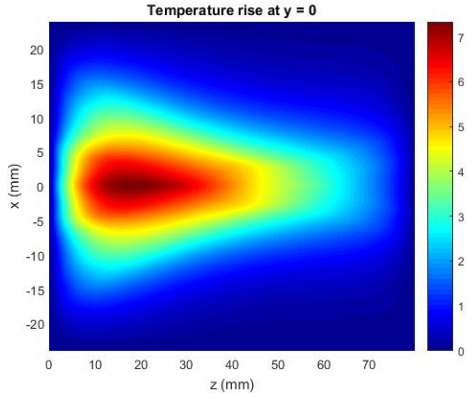

Figure 6.6 Temperature profile simulated from modified heterogeneous Rayleigh-Sommerfeld model.

6.4 Estimation Model for Heterogeneous Media

In order to estimate focused ultrasound response in heterogeneous media, ultrasound wave was focused at different distances (from 25 mm to 75 mm) and the effect of maximum responses were calculated using Rayleigh-Sommerfeld simulations. A set of standard combination of tissue layers, coupling medium (5 mm), skin (3 mm), Fat (10 mm) and Kidney/Pancreas/Viscera (82mm) are used. The tissue properties selected for simulations are listed in Table 6.1.

Table 6.1 Selected Properties of Tissues for Focused Ultrasound Simulation in Heterogeneous Media (Duck 1990, Eikelder et al. 2016, Ginter 2000, Goss et al. 1980, Gowrishankar et al. 2004, Hand et al. 1982, Jungsoon et al. 2015, Rossetto, Diederich and Stauffer 2000)

	Unit(SI)	*Coupling medium*	*Skin*	*Fat*	*Kidney*	*Pancreas*	*Visceral Tissue*	*Muscle*	*Liver*
Sp. Heat Capacity of blood	J/kg-K	3480	3480	3480	3480	3480	3480	3480	3480
Blood perfusion	Kg/m^3-s	0	5	0.54	10	10	10	2.3	15
Density	Kg/m^3	1033	1200	950	1050	1050	1060	1065	1050
Speed of sound	m/s	1490	1560	1478	1560	1591	1540	1575	1540
Power law exponent	Unitless	2	2	1.4	2	0.78	1.25	1	1
Attenuation	dB/cm-MHz	0.58	2.5	0.61	0.7	0.955	0.2779	0.575	0.39
Sp. Heat of medium	J/kg-K	3960	3400	3800	3890	3160	3160	3430	3639
Thermal Conductivity	W/m-K	0.5574	0.23	0.217	0.544	0.547	0.547	0.50	0.51
Nonlinearity parameter	Unitless	0.35	4.435	5.5	4.99	2.85	2.85	4.2	3.9

[a]Units are the same as International System Units(SI); J = Joule, kg = kilogram, K = kelvin, m = meter, s = second, dB = decibel, cm = centimeter, MHz = megahertz, W = watt .

To demonstrate the performance of proposed model in heterogeneous media, prediction profile patterns of four combined layers are selected as illustrated in Figure 6.1 and only the final tissue layer (viscera, kidney or pancreas), is replaced to establish model parameters through computer program. Prediction model function defined by Equation

(5.1) in Chapter 5, with different fitting parameters was selected to represent simulations in each combination. Figure 6.7 (a) shows maximum pressure response found for different focus depths (25 mm to 75 mm) and for different sets of tissue layer combinations. Figure 6.7 (b) shows the corresponding steady state temperature rise profiles. The optimized fitting parameters $y_0, x_c, w \; and \; A$ for heterogeneous model are selected through GA algorithm.

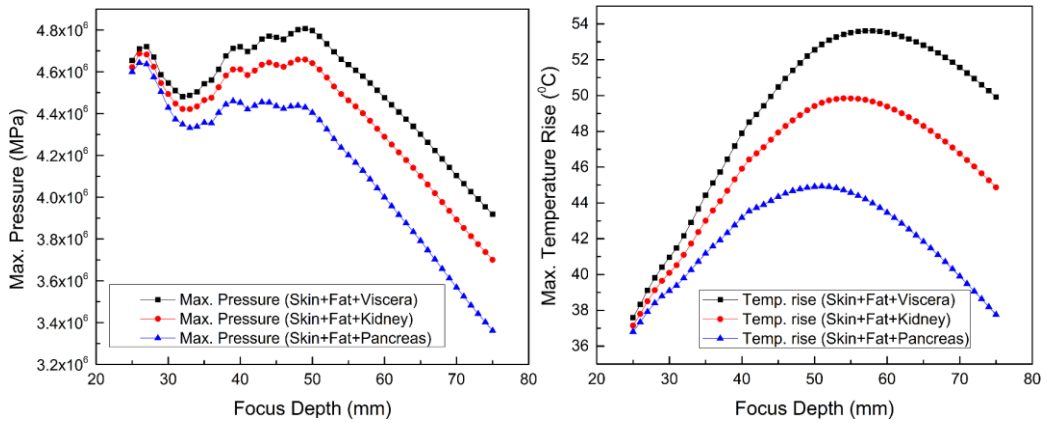

(a) (b)

Figure 6.7 (a) Maximum pressure and (b) Maximum temperature rise profile patterns for different focus depth (25 mm to 75 mm) by different sets of tissue layers. Here, 16 by 1 phased array elements with 5 cm by 1 cm transducer surface area are used.

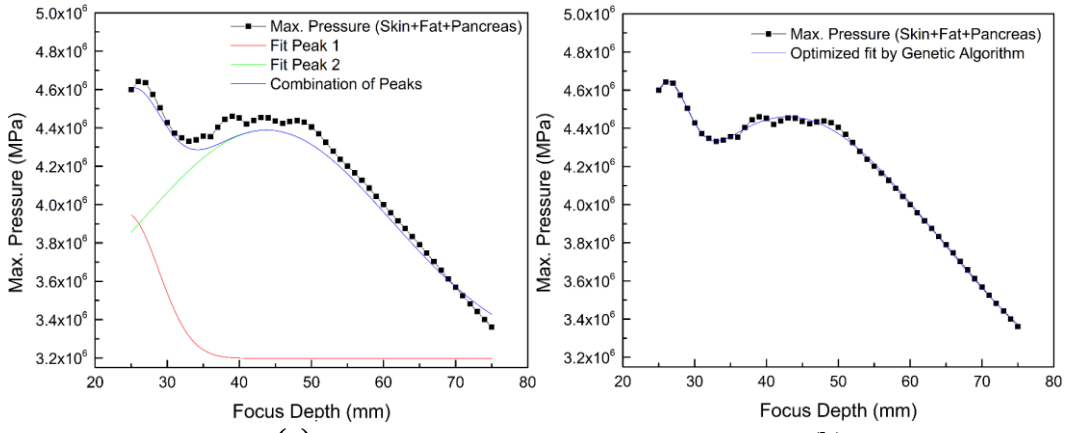

(a) (b)

Figure 6.8 (a) Combination of Gaussian profile peaks to define estimation model for maximum pressure in pancreas tissue, where coupling gel (5 mm), skin (3 mm) and fat (10 mm) tissues are used as surrounding layers. (b) Maximum pressure estimation profile obtained through GA optimization.

The steady state temperature rise is generated by solving bio-heat equation for respective pressure fields and the maximum temperature variation at variable focus zones are shown in Figure 6.9 (a). This rise pattern is modelled by using one Gaussian peak and the fitting parameters are optimized through GA. The optimized profile fitting is shown in the Figure 6.9 (b)

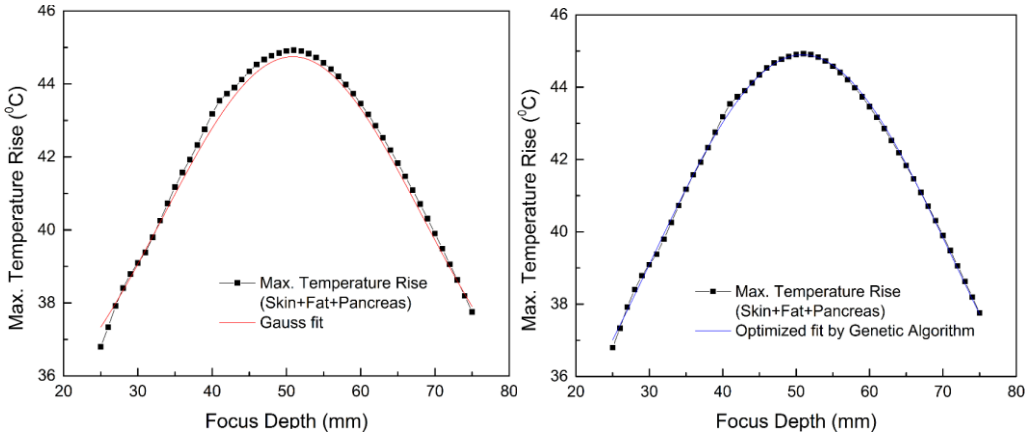

(a) (b)

Figure 6.9 (a) Gaussian estimation profile of maximum temperature rises in pancreas, where coupling gel (5 mm), skin (3 mm) and fat (10 mm) tissues are used as surrounding layers. (b) Maximum temperature rise estimation profile obtained through GA optimization.

6.5 GUI Software for Prediction Model

A Matlab based Graphical User Interface (GUI) program is developed for the prediction of maximum pressure, power deposition and temperature in heterogeneous media. The tissue layer thicknesses are selected in such a way that it can easily replicate the HIFU therapy operations inside soft tissues of human body. Four tissue layers are utilized where the first three layers, coupling gel, skin and fat are kept constant. The transducer array focuses HIFU beam after the third layer within a range from 25 mm to 75 mm. In this range maximum pressure and temperature variations are established and modeled through GA optimization. The prediction function Equation (5.1) is used to calculate the

maximum pressure, power deposition and temperature rise at the focused zone. The profile fitting parameters used for heterogenous medium are y_0, x_c, w *and* A. These parameters are optimized through GA optimization and are stored in the GUI program for model estimation and profile pattern visualization. The procedure of implementing the fast estimation model for heterogeneous media is similar to that of homogeneous medium presented in Chapter 5.

In Figure 6.10, the model presents the simulation in a heterogeneous media consisting of 5 mm coupling gel, 3 mm skin, 10 mm fat and 82 mm kidney tissue layers, where ultrasound beam is focused at a depth of 51.05 mm distance through the initial layers. Maximum pressure is 4.5844 MPa, power deposition is 642.468 kW/m^2 and temperature rise is 49.4136°C at the focused zone can be obtained instantaneously through this interface. The pressure field, power field and temperature field pattern shown in the GUI program can also be updated dynamically with the movement of focusing depth sliding bar.

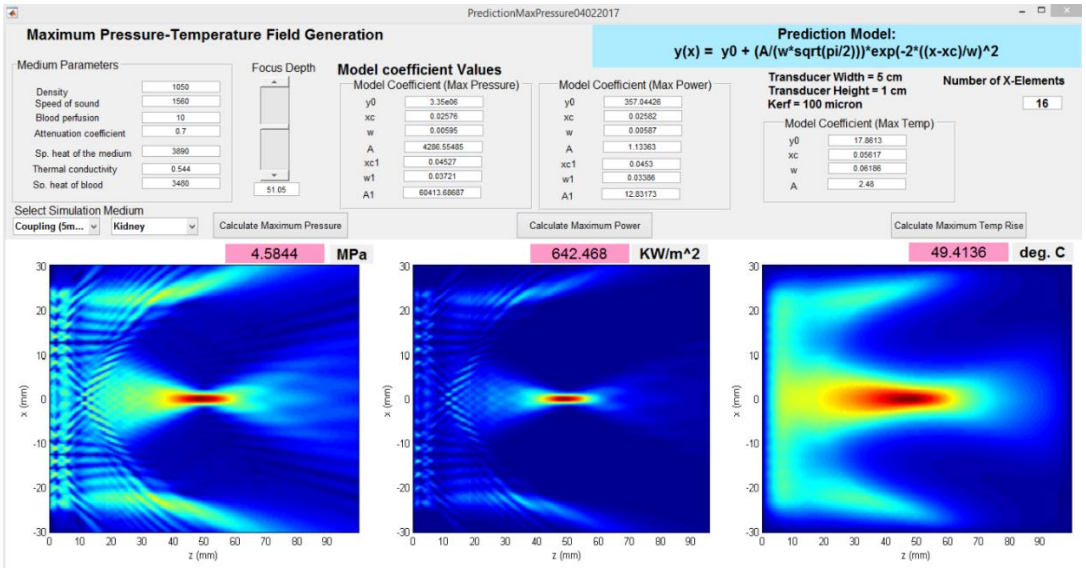

Figure 6.10 GUI program of estimation model to calculate maximum pressure, power deposition and temperature rise along with field pattern visualization.

6.6 Results and Discussion

In this study, pressure variation patterns with respect to transducer geometry and focus depth have been used to establish an estimation model which is capable to provide maximum pressure and temperature values instantaneously with a good accuracy. High frequency focused ultrasound beam simulation is typically very complex and time expensive. Therefore, a fast simulation method based on existing reference data would facilitate the process of primary estimation during medical treatment planning. Fast estimation process for heterogeneous media can also help surgeon to make quick decision through many trials on simulations.

Typically, a Rayleigh-Sommerfeld calculation for a heterogeneous media with 30 mm × 30 mm × 80 mm calculation volume takes about 40 to 50 minutes and an Angular Spectrum calculation takes 20 to 30 minutes to finish in a computer system with Intel(R) Core i7, Dual core 2.00 GHz processor and 16.0 GB memory (RAM). But these calculation times can increase significantly with the complexity of tissue position and geometry. Table 6.2 shows the performance of heterogeneous estimation model compared with Rayleigh-Sommerfeld and Angular Spectrum simulations. In this table, five random focus depths have been selected from a random point generator program and maximum pressure, power deposition and temperature rise have been evaluated in these focus distances by using the optimized model function parameters. Three different tissue media (visceral tissue, kidney tissue and pancreas tissue) have been used after initial coupling gel, skin and fat layers.

Table 6.2 Heterogeneous Prediction Model Comparison with Rayleigh-Sommerfeld and Angular Spectrum Method at Random Data Points for Visceral, Kidney and Pancreas Tissues

		Prediction Model			Rayleigh-Sommerfeld			Angular Spectrum		
	Focus Depth	Maximum Pressure	Power Deposition	Temp. Rise	Maximum Pressure	Power Deposition	Temp. Rise	Maximum Pressure	Power Deposition	Temp. Rise
Units[a]	mm	MPa	KW/m^2	°C	MPa	KW/m^2	°C	MPa	KW/m^2	°C
Visceral tissue	37.387	4.629	655.676	46.122	4.638	640.839	45.987	4.785	679.735	47.43
	59.019	4.525	626.850	53.682	4.510	702.900	53.575	4.587	633.727	54.493
	35.516	4.569	638.641	44.911	4.554	702.145	44.791	4.621	644.766	45.444
	68.298	4.161	529.666	52.185	4.170	694.011	52.047	4.254	543.32	53.091
	29.491	4.568	638.585	40.704	4.557	549.977	40.693	4.625	645.66	41.29
Average % Model Error					0.101	0.101	0.215	1.831	1.836	1.7134
Kidney tissue	54.065	4.509	621.489	49.774	4.491	615.580	49.841	4.544	622.82	50.427
	61.023	4.255	553.493	49.457	4.250	551.427	49.204	4.262	552.9	49.33
	39.381	4.582	641.491	45.467	4.614	649.810	45.544	4.681	659.31	46.21
	47.52	4.636	656.825	48.622	4.653	660.771	48.765	4.730	671.79	49.57
	42.348	4.630	654.852	46.809	4.617	650.829	46.869	4.791	675.25	48.62
Average % Model Error					0.0594	0.0085	0.0392	1.7211	1.6948	1.6525
Pancreas tissue	61.189	3.957	468.677	43.201	3.950	466.960	43.109	3.951	467.338	43.134
	45.018	4.453	593.468	44.333	4.435	588.799	44.348	4.498	605.435	45.601
	52.072	4.316	557.778	44.880	4.321	558.929	44.897	4.302	554.033	44.504
	35.535	4.368	570.743	41.408	4.357	568.176	41.401	4.489	585.404	42.656
	71.726	3.494	365.698	39.182	3.494	365.379	39.174	3.506	366.670	39.310
Average % Model Error					0.146	0.319	0.0001	0.768	0.873	1.06

[a]Units are the same as International System Units(SI); J = Joule, kg = kilogram, K = kelvin, m = meter, s = second, dB = decibel, mm = milimeter, MHz = megahertz, KW = kilowatt, MPa = Megapascal, °C = Degree Centigrade.

Average percentages of model error found for maximum pressure, power deposition and temperature rise are shown in Table 6.2. For viscera, kidney and pancreas tissue, average model error in pressure estimation compared to Rayleigh-Sommerfeld model are 0.101%, 0.0594% and 0.146%, respectively and compared to Angular Spectrum method these errors are 1.831%, 1.7211% and 0.768%, respectively. Average model error for maximum power deposition and temperature rise are also found to be minimal.

The results show that optimized heterogeneous prediction model can quickly and efficiently capture responses of focused ultrasound beam. The initial layers used in this estimation model (coupling gel, skin and fat) can be replaced by different tissue media. In that case, based on individual tissue layer properties the fitting component parameters of the model will change. This fast prediction method can also be extended for various tissue layer thicknesses and transducer geometries by adding optimized parameter components to the model.

CHAPTER 7

SUMMARY AND FUTURE WORK

7.1 Summary

In this dissertation, a method of optimizing array element distribution over the transducer surface is presented in Chapter 4. It is demonstrated that, during HIFU surgery focus intensity can be controlled by changing array element numbers in X and Y direction. Although during manufacturing of array transducer certain fixed numbers of elements are considered based on the shape of cutting dice, this study will provide a platform to manufacture array elements on transducer surface that is not conventional. For example, for an investigation area, 2.64 cm^2, the optimum number of array element found to be 210 (21 × 10). If this information can be obtained through numerical simulation before actual manufacturing, phased array arrangement can be selected in an efficient way. The idea of knowing optimum array distribution is also beneficial after manufacturing the transducer. Because a phased array transducer can be excited partially (only the optimum elements) to achieve maximum intensity at the required focus depth.

As stated in the objectives, we have presented a model for doing fast estimation of focus ultrasound surgery in Chapters 5 and 6. This model is developed for both homogeneous and heterogeneous media. One of the major obstacles to develop this model was to implement Rayleigh-Sommerfeld simulation for layered media, since it is traditionally applicable only for homogeneous media. To overcome this difficulty, a modified method for using Rayleigh-Sommerfeld model in heterogeneous media is developed and the response results found to be consistent or very close to those found

from other establish numerical models. To implement this model effectively a Genetic Algorithm is used to optimize prediction model equation parameters.

The estimation model for both homogeneous and heterogeneous media have shown minimal model error compared to Rayleigh-Sommerfeld and Angular Spectrum method. The pressure, power and temperature field pattern can be visualized in a GUI program interface with this model and the speed of this estimation model is very fast, as it calculates only a prediction model equation through Matlab programming.

7.2 Future Work

A major portion of this dissertation deals with fast estimation model that can efficiently calculate response solutions of time expensive numerical models. This model is primarily developed for phased array transducers, which is successfully applied in many clinical settings for breast and prostate cancer treatments. For tumor treatments of liver, pancreas and viscera tissue, bowl type single element transducer is widely used. However, according to many researchers, usability of phased array element in ultrasound therapy will provide more control or options on treating tumor region. Experimental validation of modified Rayleigh-Sommerfeld simulation are done in Chapter 6, which helps us to understand the effectiveness of this model for practical implementation. To further our research study, we intend to compare the responses found from estimation model to those found in literature for varying focus depths and different array distribution.

Furthermore, we plan to test the model by changing the layer thicknesses and layer properties. If the individual layer thicknesses used in heterogeneous estimation model can be replaced by arbitrary model parameters along with tissue properties, the flexibility and robustness of the model will improve significantly.

APPENDIX

MATLAB SOURCE CODES FOR GUI SOFTWARE

Matlab codes for GUI software to estimate pressure-temperature values and to visualize field pattern are as follows:

```
% GUI code for PredictionMaxPressure06272017.m
function varargout =
PredictionMaxPressure06282017(varargin)
% PREDICTIONMAXPRESSURE06282017 MATLAB code for
% Begin initialization code - DO NOT EDIT
gui_Singleton = 1;
gui_State = struct('gui_Name',       mfilename, ...
                   'gui_Singleton',  gui_Singleton, ...
                   'gui_OpeningFcn',
@PredictionMaxPressure06282017_OpeningFcn, ...
                   'gui_OutputFcn',
@PredictionMaxPressure06282017_OutputFcn, ...
                   'gui_LayoutFcn',  [] , ...
                   'gui_Callback',   []);
if nargin && ischar(varargin{1})
    gui_State.gui_Callback = str2func(varargin{1});
end

if nargout
    [varargout{1:nargout}] = gui_mainfcn(gui_State,
varargin{:});
else
    gui_mainfcn(gui_State, varargin{:});
end
% End initialization code - DO NOT EDIT


% --- Executes just before PredictionMaxPressure06282017 is
made visible.
function PredictionMaxPressure06282017_OpeningFcn(hObject,
eventdata, handles, varargin)
% This function has no output args, see OutputFcn.
handles.output = hObject;
% Update handles structure
guidata(hObject, handles);
% --- Outputs from this function are returned to the
command line.
```

```
function varargout =
PredictionMaxPressure06282017_OutputFcn(hObject, eventdata,
handles)
varargout{1} = handles.output;

% --- Executes on selection change in popupMedium.
function popupMedium_Callback(hObject, eventdata, handles)

str = get(hObject,'String');
val = get(hObject,'Value');

switch str{val};
    case 'Pancreas'
        set(handles.editDensity,'String','1050');
        set(handles.editSpeed,'String','1591');
        set(handles.editPerfusion,'String','10');
        set(handles.editAttenuation,'String','0.955');
        set(handles.editSpheat,'String','3160');
        set(handles.editConductivity,'String','0.547');
        set(handles.editSpheatBlood,'String','3480');

   case 'Viscera'
        set(handles.editDensity,'String','1060');
        set(handles.editSpeed,'String','1540');
        set(handles.editPerfusion,'String','10');
        set(handles.editAttenuation,'String','0.2779');
        set(handles.editSpheat,'String','3160');
        set(handles.editConductivity,'String','0.547');
        set(handles.editSpheatBlood,'String','3480');

    case 'Kidney'
        set(handles.editDensity,'String','1050');
        set(handles.editSpeed,'String','1560');
        set(handles.editPerfusion,'String','10');
        set(handles.editAttenuation,'String','0.7');
        set(handles.editSpheat,'String','3890');
        set(handles.editConductivity,'String','0.544');
        set(handles.editSpheatBlood,'String','3480');

     case 'Liver'
        set(handles.editDensity,'String','1050');
        set(handles.editSpeed,'String','1540');
        set(handles.editPerfusion,'String','15');
        set(handles.editAttenuation,'String','0.39087');
        set(handles.editSpheat,'String','3639');
        set(handles.editConductivity,'String','0.512');
        set(handles.editSpheatBlood,'String','3480');
```

```
    end
 % --- Executes during object creation, after setting all
properties.
function popupMedium_CreateFcn(hObject, eventdata, handles)
%       See ISPC and COMPUTER.
if ispc && isequal(get(hObject,'BackgroundColor'),
get(0,'defaultUicontrolBackgroundColor'))
    set(hObject,'BackgroundColor','white');
end



function editDensity_Callback(hObject, eventdata, handles)
function editDensity_CreateFcn(hObject, eventdata, handles)
if ispc && isequal(get(hObject,'BackgroundColor'),
get(0,'defaultUicontrolBackgroundColor'))
    set(hObject,'BackgroundColor','white');
end
function editSpeed_Callback(hObject, eventdata, handles)
function editSpeed_CreateFcn(hObject, eventdata, handles)
if ispc && isequal(get(hObject,'BackgroundColor'),
get(0,'defaultUicontrolBackgroundColor'))
    set(hObject,'BackgroundColor','white');
end
function editPerfusion_Callback(hObject, eventdata,
handles)
function editPerfusion_CreateFcn(hObject, eventdata,
handles)
if ispc && isequal(get(hObject,'BackgroundColor'),
get(0,'defaultUicontrolBackgroundColor'))
    set(hObject,'BackgroundColor','white');
end
function editAttenuation_Callback(hObject, eventdata,
handles)
function editAttenuation_CreateFcn(hObject, eventdata,
handles)
if ispc && isequal(get(hObject,'BackgroundColor'),
get(0,'defaultUicontrolBackgroundColor'))
    set(hObject,'BackgroundColor','white');
end
function editSpheat_Callback(hObject, eventdata, handles)
function editSpheat_CreateFcn(hObject, eventdata, handles)
if ispc && isequal(get(hObject,'BackgroundColor'),
get(0,'defaultUicontrolBackgroundColor'))
    set(hObject,'BackgroundColor','white');
end
```

```
function editConductivity_Callback(hObject, eventdata,
handles)
function editConductivity_CreateFcn(hObject, eventdata,
handles)
if ispc && isequal(get(hObject,'BackgroundColor'),
get(0,'defaultUicontrolBackgroundColor'))
    set(hObject,'BackgroundColor','white');
end

function editSpheatBlood_Callback(hObject, eventdata,
handles)
function editSpheatBlood_CreateFcn(hObject, eventdata,
handles)
if ispc && isequal(get(hObject,'BackgroundColor'),
get(0,'defaultUicontrolBackgroundColor'))
    set(hObject,'BackgroundColor','white');
end
% --- Executes on slider movement.
function depthSlider_Callback(hObject, eventdata, handles)

a = get(handles.depthSlider,'Value');
astr=num2str(a);
set(handles.depthText,'String',astr);

%%%%%%%%%%%%%%%%%%%%%%%%%%%%%
%The following part is for pattern display
if a>=25 && a<25.5
    b=imread('LP25.tif');
    c=imread('LW25.tif');
    d=imread('LT25.tif');
     AxesH1 = axes('Units', 'pixels', 'position', [-10, 5,
560, 460]);
     AxesH2 = axes('Units', 'pixels', 'position', [500, 5,
560, 460]);
     AxesH3 = axes('Units', 'pixels', 'position', [990, 5,
560, 460]);

   image(b,'Parent',AxesH1);
   image(c,'Parent',AxesH2);
   image(d,'Parent',AxesH3);

   axis(AxesH1,'off');
   axis(AxesH2,'off');
   axis(AxesH3,'off');

elseif  a>=25.5 && a<26
      b=imread('LP25.5.tif');
```

```
    c=imread('LW25.5.tif');
    d=imread('LT25.5.tif');
     AxesH1 = axes('Units', 'pixels', 'position', [-10, 5,
560, 460]);
     AxesH2 = axes('Units', 'pixels', 'position', [500, 5,
560, 460]);
     AxesH3 = axes('Units', 'pixels', 'position', [990, 5,
560, 460]);

   image(b,'Parent',AxesH1);
   image(c,'Parent',AxesH2);
   image(d,'Parent',AxesH3);

   axis(AxesH1,'off');
   axis(AxesH2,'off');
   axis(AxesH3,'off');

   elseif a>=26 && a<26.5
    b=imread('LP26.tif');
    c=imread('LW26.tif');
    d=imread('LT26.tif');
     AxesH1 = axes('Units', 'pixels', 'position', [-10, 5,
560, 460]);
     AxesH2 = axes('Units', 'pixels', 'position', [500, 5,
560, 460]);
     AxesH3 = axes('Units', 'pixels', 'position', [990, 5,
560, 460]);

   image(b,'Parent',AxesH1);
   image(c,'Parent',AxesH2);
   image(d,'Parent',AxesH3);

   axis(AxesH1,'off');
   axis(AxesH2,'off');
   axis(AxesH3,'off');

elseif  a>=26.5 && a<27
      b=imread('LP26.5.tif');
    c=imread('LW26.5.tif');
    d=imread('LT26.5.tif');
     AxesH1 = axes('Units', 'pixels', 'position', [-10, 5,
560, 460]);
     AxesH2 = axes('Units', 'pixels', 'position', [500, 5,
560, 460]);
     AxesH3 = axes('Units', 'pixels', 'position', [990, 5,
560, 460]);
```

```
   image(b,'Parent',AxesH1);
   image(c,'Parent',AxesH2);
   image(d,'Parent',AxesH3);

   axis(AxesH1,'off');
   axis(AxesH2,'off');
   axis(AxesH3,'off');

 elseif a>=27 && a<27.5
    b=imread('LP27.tif');
    c=imread('LW27.tif');
    d=imread('LT27.tif');
     AxesH1 = axes('Units', 'pixels', 'position', [-10, 5,
560, 460]);
     AxesH2 = axes('Units', 'pixels', 'position', [500, 5,
560, 460]);
     AxesH3 = axes('Units', 'pixels', 'position', [990, 5,
560, 460]);

   image(b,'Parent',AxesH1);
   image(c,'Parent',AxesH2);
   image(d,'Parent',AxesH3);

   axis(AxesH1,'off');
   axis(AxesH2,'off');
   axis(AxesH3,'off');

elseif  a>=27.5 && a<28
      b=imread('LP27.5.tif');
    c=imread('LW27.5.tif');
    d=imread('LT27.5.tif');
     AxesH1 = axes('Units', 'pixels', 'position', [-10, 5,
560, 460]);
     AxesH2 = axes('Units', 'pixels', 'position', [500, 5,
560, 460]);
     AxesH3 = axes('Units', 'pixels', 'position', [990, 5,
560, 460]);

   image(b,'Parent',AxesH1);
   image(c,'Parent',AxesH2);
   image(d,'Parent',AxesH3);

   axis(AxesH1,'off');
   axis(AxesH2,'off');
   axis(AxesH3,'off');

    elseif a>=28 && a<28.5
```

```
    b=imread('LP28.tif');
    c=imread('LW28.tif');
    d=imread('LT28.tif');
     AxesH1 = axes('Units', 'pixels', 'position', [-10, 5,
560, 460]);
     AxesH2 = axes('Units', 'pixels', 'position', [500, 5,
560, 460]);
     AxesH3 = axes('Units', 'pixels', 'position', [990, 5,
560, 460]);

   image(b,'Parent',AxesH1);
   image(c,'Parent',AxesH2);
   image(d,'Parent',AxesH3);

   axis(AxesH1,'off');
   axis(AxesH2,'off');
   axis(AxesH3,'off');

elseif  a>=28.5 && a<29
      b=imread('LP28.5.tif');
    c=imread('LW28.5.tif');
    d=imread('LT28.5.tif');
     AxesH1 = axes('Units', 'pixels', 'position', [-10, 5,
560, 460]);
     AxesH2 = axes('Units', 'pixels', 'position', [500, 5,
560, 460]);
     AxesH3 = axes('Units', 'pixels', 'position', [990, 5,
560, 460]);

   image(b,'Parent',AxesH1);
   image(c,'Parent',AxesH2);
   image(d,'Parent',AxesH3);

   axis(AxesH1,'off');
   axis(AxesH2,'off');
   axis(AxesH3,'off');


 elseif a>=29 && a<29.5
    b=imread('LP29.tif');
    c=imread('LW29.tif');
    d=imread('LT29.tif');
     AxesH1 = axes('Units', 'pixels', 'position', [-10, 5,
560, 460]);
     AxesH2 = axes('Units', 'pixels', 'position', [500, 5,
560, 460]);
```

```
     AxesH3 = axes('Units', 'pixels', 'position', [990, 5,
560, 460]);

   image(b,'Parent',AxesH1);
   image(c,'Parent',AxesH2);
   image(d,'Parent',AxesH3);

   axis(AxesH1,'off');
   axis(AxesH2,'off');
   axis(AxesH3,'off');

elseif  a>=29.5 && a<30
      b=imread('LP29.5.tif');
    c=imread('LW29.5.tif');
    d=imread('LT29.5.tif');
     AxesH1 = axes('Units', 'pixels', 'position', [-10, 5,
560, 460]);
     AxesH2 = axes('Units', 'pixels', 'position', [500, 5,
560, 460]);
     AxesH3 = axes('Units', 'pixels', 'position', [990, 5,
560, 460]);

   image(b,'Parent',AxesH1);
   image(c,'Parent',AxesH2);
   image(d,'Parent',AxesH3);

   axis(AxesH1,'off');
   axis(AxesH2,'off');
   axis(AxesH3,'off');
%%%%%%%
From 30 mm to 74 mm focus distance pattern display codes
are written in similar fashion and this portion is excluded
from the appendix. From 74 mm to 75 mm pattern display
codes are shown below.
%%%%%%


elseif   a>=74 && a<74.5
     b=imread('LP74.tif');
    c=imread('LW74.tif');
    d=imread('LT74.tif');
     AxesH1 = axes('Units', 'pixels', 'position', [-10, 5,
560, 460]);
     AxesH2 = axes('Units', 'pixels', 'position', [500, 5,
560, 460]);
     AxesH3 = axes('Units', 'pixels', 'position', [990, 5,
560, 460]);
```

```
   image(b,'Parent',AxesH1);
   image(c,'Parent',AxesH2);
   image(d,'Parent',AxesH3);

   axis(AxesH1,'off');
   axis(AxesH2,'off');
   axis(AxesH3,'off');

elseif   a>=74.5 && a<75
     b=imread('LP74.5.tif');
    c=imread('LW74.5.tif');
    d=imread('LT74.5.tif');
     AxesH1 = axes('Units', 'pixels', 'position', [-10, 5,
560, 460]);
     AxesH2 = axes('Units', 'pixels', 'position', [500, 5,
560, 460]);
     AxesH3 = axes('Units', 'pixels', 'position', [990, 5,
560, 460]);

   image(b,'Parent',AxesH1);
   image(c,'Parent',AxesH2);
   image(d,'Parent',AxesH3);

   axis(AxesH1,'off');
   axis(AxesH2,'off');
   axis(AxesH3,'off');

   %%%%%%%%%%%%%%%%%%
else    a = 75
      b=imread('LP75.tif');
    c=imread('LW75.tif');
    d=imread('LT75.tif');
     AxesH1 = axes('Units', 'pixels', 'position', [-10, 5,
560, 460]);
     AxesH2 = axes('Units', 'pixels', 'position', [500, 5,
560, 460]);
     AxesH3 = axes('Units', 'pixels', 'position', [990, 5,
560, 460]);

   image(b,'Parent',AxesH1);
   image(c,'Parent',AxesH2);
   image(d,'Parent',AxesH3);

   axis(AxesH1,'off');
   axis(AxesH2,'off');
   axis(AxesH3,'off');
```

```
end

% set model parameters for calculating temperature rise.

        set(handles.edity0t,'String',' 17.8613');
        set(handles.editxct,'String','0.05617');
        set(handles.editwt,'String','0.06186');
        set(handles.editAt,'String','2.48');

% set model parameters for maximum pressure calculation.

        set(handles.edity0,'String','3.35e06');
        set(handles.editxc,'String','0.02576');
        set(handles.editw,'String','0.00595');
        set(handles.editA,'String','4286.55485');

        set(handles.editxc1,'String','0.04527');
        set(handles.editw1,'String','0.03721');
        set(handles.editA1,'String','60413.68687');

% set model parameters for maximum power deposition
%calculation.

        set(handles.edity0p,'String','357.04426');
        set(handles.editxcp,'String','0.02582');
        set(handles.editwp,'String','0.00587');
        set(handles.editAp,'String','1.13363');

        set(handles.editxc1p,'String','0.0453');
        set(handles.editw1p,'String','0.03386');
        set(handles.editA1p,'String','12.83173');


function depthSlider_CreateFcn(hObject, eventdata, ~)
if isequal(get(hObject,'BackgroundColor'),
get(0,'defaultUicontrolBackgroundColor'))
    set(hObject,'BackgroundColor',[.9 .9 .9]);
end

function depthText_Callback(hObject, eventdata, handles)
astr=get(handles.depthText,'String');
a = str2double(astr);
set(handles.depthSlider,'Value',a);

function depthText_CreateFcn(hObject, eventdata, handles)
```

```
if ispc && isequal(get(hObject,'BackgroundColor'),
get(0,'defaultUicontrolBackgroundColor'))
    set(hObject,'BackgroundColor','white');

end
function ShowGeneralModel_CreateFcn(hObject, eventdata,
handles)
function edity0_Callback(hObject, eventdata, handles)
function edity0_CreateFcn(hObject, eventdata, handles)
if ispc && isequal(get(hObject,'BackgroundColor'),
get(0,'defaultUicontrolBackgroundColor'))
    set(hObject,'BackgroundColor','white');
end
function editxc_Callback(hObject, eventdata, handles)
function editxc_CreateFcn(hObject, eventdata, handles)
if ispc && isequal(get(hObject,'BackgroundColor'),
get(0,'defaultUicontrolBackgroundColor'))
    set(hObject,'BackgroundColor','white');
end

function editb1_Callback(hObject, eventdata, handles)
function editb1_CreateFcn(hObject, eventdata, handles)
if ispc && isequal(get(hObject,'BackgroundColor'),
get(0,'defaultUicontrolBackgroundColor'))
    set(hObject,'BackgroundColor','white');
end
function editA_Callback(hObject, eventdata, handles)
function editA_CreateFcn(hObject, eventdata, handles)
if ispc && isequal(get(hObject,'BackgroundColor'),
get(0,'defaultUicontrolBackgroundColor'))
    set(hObject,'BackgroundColor','white');
end

function editb2_Callback(hObject, eventdata, handles)
function editb2_CreateFcn(hObject, eventdata, handles)
if ispc && isequal(get(hObject,'BackgroundColor'),
get(0,'defaultUicontrolBackgroundColor'))
    set(hObject,'BackgroundColor','white');
end

function edita3_Callback(hObject, eventdata, handles)
function edita3_CreateFcn(hObject, eventdata, handles)
if ispc && isequal(get(hObject,'BackgroundColor'),
get(0,'defaultUicontrolBackgroundColor'))
    set(hObject,'BackgroundColor','white');
end
function editb3_Callback(hObject, eventdata, handles)
```

```
function editb3_CreateFcn(hObject, eventdata, handles)
if ispc && isequal(get(hObject,'BackgroundColor'),
get(0,'defaultUicontrolBackgroundColor'))
    set(hObject,'BackgroundColor','white');
end
function editw_Callback(hObject, eventdata, handles)
function editw_CreateFcn(hObject, eventdata, handles)
if ispc && isequal(get(hObject,'BackgroundColor'),
get(0,'defaultUicontrolBackgroundColor'))
    set(hObject,'BackgroundColor','white');
end

% --- Executes on button press in pushbutton1.
function pushbutton1_Callback(hObject, eventdata, handles)

%% calculate prediction model function

ShowMaxPressureKidney25to75(handles);

function axes1_CreateFcn(hObject, eventdata, handles)
function edity0p_Callback(hObject, eventdata, handles)
function edity0p_CreateFcn(hObject, eventdata, handles)
if ispc && isequal(get(hObject,'BackgroundColor'),
get(0,'defaultUicontrolBackgroundColor'))
    set(hObject,'BackgroundColor','white');
end

function editxcp_Callback(hObject, eventdata, handles)
function editxcp_CreateFcn(hObject, eventdata, handles)
if ispc && isequal(get(hObject,'BackgroundColor'),
get(0,'defaultUicontrolBackgroundColor'))
    set(hObject,'BackgroundColor','white');
end
function editAp_Callback(hObject, eventdata, handles)
function editAp_CreateFcn(hObject, eventdata, handles)
if ispc && isequal(get(hObject,'BackgroundColor'),
get(0,'defaultUicontrolBackgroundColor'))
    set(hObject,'BackgroundColor','white');
end
function editwp_Callback(hObject, eventdata, handles)
function editwp_CreateFcn(hObject, eventdata, handles)
if ispc && isequal(get(hObject,'BackgroundColor'),
get(0,'defaultUicontrolBackgroundColor'))
    set(hObject,'BackgroundColor','white');
end
function pushbutton2_Callback(hObject, eventdata, handles)
%% calculate prediction model function
```

```
ShowMaxPowerKidney25to75(handles);

function textMaxPower_CreateFcn(hObject, eventdata,
handles)
function edity0t_Callback(hObject, eventdata, handles)
function edity0t_CreateFcn(hObject, eventdata, handles)
if ispc && isequal(get(hObject,'BackgroundColor'),
get(0,'defaultUicontrolBackgroundColor'))
    set(hObject,'BackgroundColor','white');
end
function editxct_Callback(hObject, eventdata, handles)
function editxct_CreateFcn(hObject, eventdata, handles)
if ispc && isequal(get(hObject,'BackgroundColor'),
get(0,'defaultUicontrolBackgroundColor'))
    set(hObject,'BackgroundColor','white');
end
function editAt_Callback(hObject, eventdata, handles)
function editAt_CreateFcn(hObject, eventdata, handles)
if ispc && isequal(get(hObject,'BackgroundColor'),
get(0,'defaultUicontrolBackgroundColor'))
    set(hObject,'BackgroundColor','white');
end
function editwt_Callback(hObject, eventdata, handles)
function editwt_CreateFcn(hObject, eventdata, handles)
if ispc && isequal(get(hObject,'BackgroundColor'),
get(0,'defaultUicontrolBackgroundColor'))
    set(hObject,'BackgroundColor','white');
end


function pushbutton3_Callback(hObject, eventdata, handles)

%% Calculate prediction model function

ShowMaxTempRiseKidney25to75(handles);
function textMaxPressure_CreateFcn(hObject, eventdata,
handles)
function edit26_Callback(hObject, eventdata, handles)
function edit26_CreateFcn(hObject, eventdata, handles)
if ispc && isequal(get(hObject,'BackgroundColor'),
get(0,'defaultUicontrolBackgroundColor'))
    set(hObject,'BackgroundColor','white');
end

function editA1_Callback(hObject, eventdata, handles)
function editA1_CreateFcn(hObject, eventdata, handles)
```

```
if ispc && isequal(get(hObject,'BackgroundColor'),
get(0,'defaultUicontrolBackgroundColor'))
    set(hObject,'BackgroundColor','white');
end

function editw1_Callback(hObject, eventdata, handles)
function editw1_CreateFcn(hObject, eventdata, handles)
if ispc && isequal(get(hObject,'BackgroundColor'),
get(0,'defaultUicontrolBackgroundColor'))
    set(hObject,'BackgroundColor','white');
end
function editxc1_Callback(hObject, eventdata, handles)
function editxc1_CreateFcn(hObject, eventdata, handles)
if ispc && isequal(get(hObject,'BackgroundColor'),
get(0,'defaultUicontrolBackgroundColor'))
    set(hObject,'BackgroundColor','white');
end

function editxc1p_Callback(hObject, eventdata, handles)
function editxc1p_CreateFcn(hObject, eventdata, handles)
if ispc && isequal(get(hObject,'BackgroundColor'),
get(0,'defaultUicontrolBackgroundColor'))
    set(hObject,'BackgroundColor','white');
end

function editA1p_Callback(hObject, eventdata, handles)
function editA1p_CreateFcn(hObject, eventdata, handles)
if ispc && isequal(get(hObject,'BackgroundColor'),
get(0,'defaultUicontrolBackgroundColor'))
    set(hObject,'BackgroundColor','white');
end
function editw1p_Callback(hObject, eventdata, handles)
function editw1p_CreateFcn(hObject, eventdata, handles)
if ispc && isequal(get(hObject,'BackgroundColor'),
get(0,'defaultUicontrolBackgroundColor'))
    set(hObject,'BackgroundColor','white');
end

function popupmenu2_Callback(hObject, eventdata, handles)
function popupmenu2_CreateFcn(hObject, eventdata, handles)
if ispc && isequal(get(hObject,'BackgroundColor'),
get(0,'defaultUicontrolBackgroundColor'))
    set(hObject,'BackgroundColor','white');
end
function uipanel1_CreateFcn(hObject, eventdata, handles)
```

```
% prediction model function examples are shown for
%heterogeneous kidney model.
%following codes show the maximum pressure generated
%through prediction model function for Kidney.

function ShowMaxPressureKidney25to75(handles)

      x = (get(handles.depthSlider,'Value'))/1000;

      y0 = str2double(get(handles.edity0,'String'));
      xc = str2double(get(handles.editxc,'String'));
      w = str2double(get(handles.editw,'String'));
      A = str2double(get(handles.editA,'String'));

      xc1 = str2double(get(handles.editxc1,'String'));
      w1 = str2double(get(handles.editw1,'String'));
      A1 = str2double(get(handles.editA1,'String'));

max =  y0 + (A/(w*sqrt(pi/2)))*exp(-2*((x-
xc)/w)^2)+(A1/(w1*sqrt(pi/2)))*exp(-2*((x-xc1)/w1)^2);
      maxPressure=max/1e6;


set(handles.textMaxPressure,'String',num2str(maxPressure));

function ShowMaxPowerKidney25to75(handles)

% following codes show the maximum power generated through
prediction model function for Kidney.


      x = (get(handles.depthSlider,'Value'))/1000;

      y0 = str2double(get(handles.edity0p,'String'));
      xc = str2double(get(handles.editxcp,'String'));
      w = str2double(get(handles.editwp,'String'));
      A = str2double(get(handles.editAp,'String'));

      xc1 = str2double(get(handles.editxc1p,'String'));
      w1 = str2double(get(handles.editw1p,'String'));
      A1 = str2double(get(handles.editA1p,'String'));



      max =  y0 + (A/(w*sqrt(pi/2)))*exp(-2*((x-
xc)/w)^2)+(A1/(w1*sqrt(pi/2)))*exp(-2*((x-xc1)/w1)^2);
      maxPower=max;
```

```
   set(handles.textMaxPower,'String',num2str(maxPower));

% following codes show the maximum temperature generated
through prediction model function for Kidney.

function ShowMaxTempRiseKidney25to75(handles)

      x = (get(handles.depthSlider,'Value'))/1000;

      y0 = str2double(get(handles.edity0t,'String'));
      xc = str2double(get(handles.editxct,'String'));
      w = str2double(get(handles.editwt,'String'));
      A = str2double(get(handles.editAt,'String'));


       maxTemp =  y0 + (A/(w*sqrt(pi/2)))*exp(-2*((x-
xc)/w)^2);


set(handles.textMaxTempRise,'String',num2str(maxTemp));
```

REFERENCES

Arditi, M., Foster, F. S. and Hunt, J. W. (1981). "Transient fields of concave annular arrays." Ultrasonic Imaging, **3**(1): 37-61.

Ballato, A. (1995). "Piezoelectricity: old effect, new thrusts." IEEE Transactions on Ultrasonics, Ferroelectrics, and Frequency Control, **42**(5): 916-926.

Berriet, R. and Fleury, G. (2007). "P5J-3 Design of a Piezocomposite Matrix Transducer Configuration for Multi-Mode Operation in HIFU Applications." Ultrasonics Symposium, 2007. IEEE, NY, USA.

Bouchoux, G., Lafon, C., Berriet, R., Chapelon, J. Y., Fleury, G. and Cathignol, D. (2008). "Dual-mode ultrasound transducer for image-guided interstitial thermal therapy." Ultrasound in Medicine & Biology, **34**(4): 607-616.

Canney, M. S., Khokhlova, V. A., Bessonova, O. V., Bailey, M. R. and Crum, L. A. (2010). "Shock-induced heating and millisecond boiling in gels and tissue due to high intensity focused ultrasound." Ultrasound in Medicine & Biology, **36**(2): 250.

Catane, R., Beck, A., Inbar, Y., Rabin, T., Shabshin, N., Hengst, S., Pfeffer, R. M., Hanannel, A., Dogadkin, O., Liberman, B. and Kopelman, D. (2007). "MR-guided focused ultrasound surgery (MRgFUS) for the palliation of pain in patients with bone metastases--preliminary clinical experience." Annals of Oncology : Official Journal of the European Society for Medical Oncology, **18**(1): 163-167.

Chapelon, J. Y., Cathignol, D., Cain, C., Ebbini, E., Kluiwstra, J. U., Sapozhnikov, O. A., Fleury, G., Berriet, R., Chupin, L. and Guey, J. L. (2000). "New piezoelectric transducers for therapeutic ultrasound." Ultrasound in Medicine & Biology, **26**(1): 153-159.

Chen, D., Kelly, J. F. and McGough, R. J. (2006). "A fast near-field method for calculations of time-harmonic and transient pressures produced by triangular pistons." The Journal of the Acoustical Society of America, **120**(5 Pt 1): 2450-2459.

Chen, D. and McGough, R. J. (2008). "A 2D fast near-field method for calculating near-field pressures generated by apodized rectangular pistons." The Journal of the Acoustical Society of America, **124**(3): 1526-1537.

Christoffersen, C., Wong, W., Pichardo, S., Togtema, G. and Curiel, L. (2016). "Class-DE Ultrasound Transducer Driver for HIFU Therapy." IEEE Transactions on Biomedical Circuits and Systems, **10**(2): 375-382.

Christopher, P. T. and Parker, K. J. (1991). "New approaches to the linear propagation of acoustic fields." The Journal of the Acoustical Society of America, **90**(1): 507-521.

Clement, G. T. and Hynynen, K. (2000). "Field characterization of therapeutic ultrasound phased arrays through forward and backward planar projection." The Journal of the Acoustical Society of America, **108**(1): 441-446.

Corry, P. M., Spanos, W. J., Tilchen, E. J., Barlogie, B., Barkley, H. T. and Armour, E. P. (1982). "Combined ultrasound and radiation therapy treatment of human superficial tumors." Radiology, **145**(1): 165-169.

Damianou, C. and Hynynen, K. (1993). "Focal spacing and near-field heating during pulsed high temperature ultrasound therapy." Ultrasound in Medicine & Biology, **19**(9): 777-787.

Daum, D. R. and Hynynen, K. (1998). "Thermal dose optimization via temporal switching in ultrasound surgery." IEEE Transactions on Ultrasonics, Ferroelectrics, and Frequency Control, **45**(1): 208-215.

Dong-Lai, L. and Waag, R. C. (1997). "Propagation and backpropagation for ultrasonic wavefront design." IEEE Transactions on Ultrasonics, Ferroelectrics, and Frequency Control, **44**(1): 1-13.

Duck, F. A. (2002). "Nonlinear acoustics in diagnostic ultrasound." Ultrasound in Medicine & Biology, **28**(1): 1-18.

Ebbini, E. S. and Cain, C. A. (1989). "Multiple-focus ultrasound phased-array pattern synthesis: optimal driving-signal distributions for hyperthermia." IEEE Transactions on Ultrasonics, Ferroelectrics, and Frequency Control, **36**(5): 540-548.

Ebbini, E. S. and Cain, C. A. (1991). "A spherical-section ultrasound phased array applicator for deep localized hyperthermia." IEEE Transactions on Bio-medical Engineering, **38**(7): 634-643.

Ebbini, E. S., Umemura, S. I., Ibbini, M. and Cain, C. A. (1988). "A cylindrical-section ultrasound phased-array applicator for hyperthermia cancer therapy." IEEE Transactions on Ultrasonics, Ferroelectrics, and Frequency Control, **35**(5): 561-572.

Fan, X. and Hynynen, K. (1995). "Control of the necrosed tissue volume during noninvasive ultrasound surgery using a 16-element phased array." Medical Physics, **22**(3): 297-306.

Fan, X. and Hynynen, K. (1996). "Ultrasound surgery using multiple sonications--treatment time considerations." Ultrasound in Medicine & Biology, **22**(4): 471-482.

Foster, F. S., Ryan, L. K. and Turnbull, D. H. (1991). "Characterization of lead zirconate titanate ceramics for use in miniature high-frequency (20-80 MHz) transducers." IEEE Transactions on Ultrasonics, Ferroelectrics, and Frequency Control, **38**(5): 446-453.

Fry, W. J., Barnard, J. W., Fry, E. J., Krumins, R. F. and Brennan, J. F. (1955). "Ultrasonic lesions in the mammalian central nervous system." Science (New York, N.Y.), **122**(3168): 517-518.

Furusawa, H., Namba, K., Nakahara, H., Tanaka, C., Yasuda, Y., Hirabara, E., Imahariyama, M. and Komaki, K. (2007). "The evolving non-surgical ablation of breast cancer: MR guided focused ultrasound (MRgFUS)." Breast Cancer, **14**(1): 55-58.

Gianfelice, D., Gupta, C., Kucharczyk, W., Bret, P., Havill, D. and Clemons, M. (2008). "Palliative treatment of painful bone metastases with MR imaging-guided focused ultrasound." Radiology, **249**(1): 355-363.

Goodman, J. W. (1996). "Introduction to Fourier Optics." McGraw-Hill.

Haller, M. I. and Khuri-Yakub, B. T. (1996). "A surface micromachined electrostatic ultrasonic air transducer." IEEE Transactions on Ultrasonics, Ferroelectrics, and Frequency Control, **43**(1): 1-6.

Hamilton, M. F. and Blackstock, D. T. (1998). "Nonlinear Acoustics." Academic Press.

Hand, J. W. and James, J. R. (1986). "Physical techniques in clinical hyperthermia." Research Studies Press.

Hill, C. R. (2005). "Generation and Structure of Acoustic Fields." Physical Principles of Medical Ultrasonics, John Wiley & Sons, Ltd**:** 41-68.

Hong, W., Aarsvold, J., O'Donnell, M. and Cain, C. (1999). "Thermal dose optimization for ultrasound tissue ablation." IEEE Transactions on Ultrasonics, Ferroelectrics, and Frequency Control, **46**(4): 913-928.

Huber, P. E., Jenne, J. W., Rastert, R., Simiantonakis, I., Sinn, H. P., Strittmatter, H. J., von Fournier, D., Wannenmacher, M. F. and Debus, J. (2001). "A new

noninvasive approach in breast cancer therapy using magnetic resonance imaging-guided focused ultrasound surgery." Cancer Research, **61**(23): 8441-8447.

Hutchins, D. A., Mair, H. D., Puhach, P. A. and Osei, A. J. (1986). "Continuous-wave pressure fields of ultrasonic transducers." The Journal of the Acoustical Society of America, **80**(1): 1-12.

Hynynen, K. (1991). "The role of nonlinear ultrasound propagation during hyperthermia treatments." Medical Physics, **18**(6): 1156-1163.

Illing, R. O., Kennedy, J. E., Wu, F., ter Haar, G. R., Protheroe, A. S., Friend, P. J., Gleeson, F. V., Cranston, D. W., Phillips, R. R. and Middleton, M. R. (2005). "The safety and feasibility of extracorporeal high-intensity focused ultrasound (HIFU) for the treatment of liver and kidney tumours in a Western population." British Journal of Cancer, **93**(8): 890-895.

J. A. Archer-Hall, A. I. B., A. J. Hazelwood (1979). "Means for computing the Kirchhoff surface integral for a disk radiator as a single integral with fixed limits." The Journal of Acoustical Society of America, **65**: 1568-1570.

Jensen, J. r. A. (1999). "A new calculation procedure for spatial impulse responses in ultrasound." The Journal of the Acoustical Society of America, **105**(6): 3266-3274.

Kelly, J. F. and McGough, R. J. (2006). "A time-space decomposition method for calculating the nearfield pressure generated by a pulsed circular piston." IEEE Transactions on Ultrasonics, Ferroelectrics, and Frequency Control, **53**(6): 1150-1159.

Kennedy, J. E., Ter Haar, G. R. and Cranston, D. (2003). "High intensity focused ultrasound: surgery of the future?" British Journal of Radiology, **76**(909): 590-599.

Kennedy, J. E., Wu, F., ter Haar, G. R., Gleeson, F. V., Phillips, R. R., Middleton, M. R. and Cranston, D. (2004). "High-intensity focused ultrasound for the treatment of liver tumours." Ultrasonics, **42**(1-9): 931-935.

Khuri-Yakub, B. T. and Oralkan, Ö. (2011). "Capacitive micromachined ultrasonic transducers for medical imaging and therapy." Journal of Micromechanics and Microengineering : Structures, Devices and Systems, **21**(5): 054004-054014.

Kinsler, L. E. (2000). "Fundamentals of Acoustics." John Wiley & Sons Australia, Limited.

Laura, P. A. (1971). "Comments on “Beam Behavior within the Nearfield of a Vibrating Piston” [J . Zemanek, J. Acoust. Soc. Amer. 49, 181–188 (1971)]." The Journal of the Acoustical Society of America, **50**(5B): 1381-1381.

Lee, L. A., Simon, C., Bove, E. L., Mosca, R. S., Ebbini, E. S., Abrams, G. D. and Ludomirsky, A. (2000). "High intensity focused ultrasound effect on cardiac tissues: potential for clinical application." Echocardiography (Mount Kisco, N.Y.), **17**(6 Pt 1): 563-566.

Leslie, T., Ritchie, R., Illing, R., Ter Haar, G., Phillips, R., Middleton, M., Bch, B., Wu, F. and Cranston, D. (2012). "High-intensity focused ultrasound treatment of liver tumours: post-treatment MRI correlates well with intra-operative estimates of treatment volume." British Journal of Radiology, **85**(1018): 1363-1370.

Liberman, B., Gianfelice, D., Inbar, Y., Beck, A., Rabin, T., Shabshin, N., Chander, G., Hengst, S., Pfeffer, R., Chechick, A., Hanannel, A., Dogadkin, O. and Catane, R. (2009). "Pain palliation in patients with bone metastases using MR-guided focused ultrasound surgery: a multicenter study." Annals of Surgical Oncology, **16**(1): 140-146.

Lindstrom, P. A. (1954). "Prefrontal ultrasonic irradiation-a substitute for lobotomy." A.M.A. Archives of Neurology and Psychiatry, **72**(4): 399-425.

Lizzi, F. L., Coleman, D. J., Driller, J., Ostromogilsky, M., Stanley, C. and Greenall, P. (1984). "Ultrasonic Hyperthermia for Ophthalmic Therapy." IEEE Transactions on Sonics and Ultrasonics, **31**(5): 473-481.

Lockwood, J. C. and Willette, J. G. (1973). "High-speed method for computing the exact solution for the pressure variations in the nearfield of a baffled piston." The Journal of the Acoustical Society of America, **53**(3): 735-741.

Madani, K., Khanmohammadi, S. and Azimirad, V. (2016). "Finding Optimal Actuation Configuration for Magnetically Driven Capsule Endoscopy Based on Genetic Algorithm." Journal of Medical and Biological Engineering, **36**(6): 776-787.

Mahesh, M. (2013). "The Essential Physics of Medical Imaging, Third Edition." Medical Physics, **40**(7): 077301.

McGough, R. J. (2004). "Rapid calculations of time-harmonic nearfield pressures produced by rectangular pistons." The Journal of the Acoustical Society of America, **115**(5 Pt 1): 1934-1941.

McGough, R. J., Ebbini, E. S. and Cain, C. A. (1992). "Direct computation of ultrasound phased-array driving signals from a specified temperature distribution for hyperthermia." IEEE Transactions on Bio-medical Engineering, **39**(8): 825-835.

McGough, R. J., Samulski, T. V. and Kelly, J. F. (2004). "An efficient grid sectoring method for calculations of the near-field pressure generated by a circular piston." The Journal of the Acoustical Society of America, **115**(5 Pt 1): 1942-1954.

Meurant, G. (1981). "Ultrasonics." Elsevier Science.

Mills, D. M. (2004). "Medical imaging with capacitive micromachined ultrasound transducer (cMUT) arrays." Ultrasonics Symposium, 2004. IEEE, Montreal, Quebec, Canada.

Moros, E. G., Roemer, R. B. and Hynynen, K. (1988). "Simulations of scanned focused ultrasound hyperthermia. the effects of scanning speed and pattern on the temperature fluctuations at the focal depth." IEEE Transactions on Ultrasonics, Ferroelectrics, and Frequency Control, **35**(5): 552-560.

Mould, J. C., Wojcik, G. L., Carcione, L. M., Tabei, M., Mast, T. D. and Waag, R. C. (1999). "Validation of FFT-based algorithms for large-scale modeling of wave propagation in tissue." Ultrasonics Symposium, 1999. IEEE, NV, USA.

Napoli, A., Anzidei, M., Ciolina, F., Marotta, E., Cavallo Marincola, B., Brachetti, G., Di Mare, L., Cartocci, G., Boni, F., Noce, V., Bertaccini, L. and Catalano, C. (2013). "MR-guided high-intensity focused ultrasound: current status of an emerging technology." Cardiovascular and Interventional Radiology, **36**(5): 1190-1203.

Oberhettinger, F. (1961). "On transient solutions of the 'baffled piston' problem." Journal of Research of the National Bureau of Standards-B. Mathematics and Mathematical Physics, **65B**(1): 1-6.

Ocheltree, K. B. and Frizzel, L. A. (1989). "Sound field calculation for rectangular sources." IEEE Transactions on Ultrasonics, Ferroelectrics, and Frequency Control, **36**(2): 242-248.

Ocheltree, K. B. and Frizzell, L. A. (1987). "Determination of power deposition patterns for localized hyperthermia: a steady-state analysis." International Journal of Hyperthermia : The Official Journal of European Society for Hyperthermic Oncology, North American Hyperthermia Group, **3**(3): 269-279.

Orofino, D. P. and Pedersen, P. C. (1993). "Efficient angular spectrum decomposition of acoustic sources. II. Results." IEEE Transactions on Ultrasonics, Ferroelectrics, and Frequency Control, **40**(3): 250-257.

Pennes, H. H. (1948). "Analysis of Tissue and Arterial Blood Temperatures in the Resting Human Forearm." Journal of Applied Physiology, **1**(2): 93-122.

Pernot, M., Aubry, J. F., Tanter, M., Thomas, J. L. and Fink, M. (2003). "High power transcranial beam steering for ultrasonic brain therapy." Physics in Medicine and Biology, **48**(16): 2577-2589.

Rangel-Merino, A., López-Bonilla, J. L. and Miranda, R. L. Y. (2005). "Optimization method based on genetic algorithms." Apeiron, **12**(4): 393-406.

Roemer, R. B. (1999). "Engineering aspects of hyperthermia therapy." Annual Review of Biomedical Engineering, **1**: 347-376.

Salgaonkar, V. A., Prakash, P., Plata, J., Holbrook, A., Rieke, V., Kurhanewicz, J., Hsu, I. C. and Diederich, C. J. (2013). "Targeted hyperthermia in prostate with an MR-guided endorectal ultrasound phased array: patient specific modeling and preliminary experiments." Proceedings of SPIE, Energy-Based Treatment of Tissue and Assessment VIII, CA, USA.

Salomir, R., Palussiere, J., Vimeux, F. C., de Zwart, J. A., Quesson, B., Gauchet, M., Lelong, P., Pergrale, J., Grenier, N. and Moonen, C. T. (2000). "Local hyperthermia with MR-guided focused ultrasound: spiral trajectory of the focal point optimized for temperature uniformity in the target region." Journal of Magnetic Resonance Imaging : JMRI, **12**(4): 571-583.

Shim, M. B. and Kim, S. J. (2014). "A sparse-element phased array system based on sequentially multiple focusing for the treatment of large tumors." IEEE International Ultrasonics Symposium, IUS, IL, USA.

Silk, M. G. (1984). "Ultrasonic Transducers for Nondestructive Testing." Taylor & Francis.

Soh, H. T., Ladabaum, I., Atalar, A., Quate, C. F. and Khuri-Yakub, B. T. (1996). "Silicon micromachined ultrasonic immersion transducers." Applied Physics Letters, **69**(24): 3674-3676.

Stepanishen, P. R. (1971). "Transient Radiation from Pistons in an Infinite Planar Baffle." The Journal of the Acoustical Society of America, **49**(5B): 1629-1638.

Sung, H. Y., Cho, S. H., Kim, J. I., Cheung, D. Y., Han, J. Y., Kim, J. K., Woo, I. S., Jung, S. E., Hahn, S. T. and Lee, Y. S. (2008). "High intensity focused ultrasound therapy resulted in a complete response in a patient with advanced gastric cancer with liver metastases: a case report." European Journal of Gastroenterology & Hepatology, **20**(7): 707-709.

Szabo, T. L. (2014). "Chapter 3 - Acoustic Wave Propagation." Diagnostic Ultrasound Imaging: Inside Out (Second Edition). Boston, Academic Press**:** 55-80.

Wojcik, G. L. and Abboud, N. (1993). "Electromechanical modeling using explicit time-domain finite elements." Ultrasonics Symposium, 1993. IEEE.

Wong, S. H., Watkins, R. D., Kupnik, M., Pauly, K. B. and Khuri-Yakub, B. T. (2008). "Feasibility of MR-temperature mapping of ultrasonic heating from a CMUT." IEEE Transactions on Ultrasonics, Ferroelectrics, and Frequency Control, **55**(4): 811-818.

Wu, F., Wang, Z. B., Cao, Y. D., Zhu, X. Q., Zhu, H., Chen, W. Z. and Zou, J. Z. (2007). ""Wide local ablation" of localized breast cancer using high intensity focused ultrasound." Journal of Surgical Oncology, **96**(2): 130-136.

Wu, F., Wang, Z. B., Chen, W. Z., Zhu, H., Bai, J., Zou, J. Z., Li, K. Q., Jin, C. B., Xie, F. L. and Su, H. B. (2004). "Extracorporeal high intensity focused ultrasound ablation in the treatment of patients with large hepatocellular carcinoma." Annals of Surgical Oncology, **11**(12): 1061-1069.

Wu, F., Wang, Z. B., Zhu, H., Chen, W. Z., Zou, J. Z., Bai, J., Li, K. Q., Jin, C. B., Xie, F. L. and Su, H. B. (2005). "Extracorporeal high intensity focused ultrasound treatment for patients with breast cancer." Breast Cancer Research and Treatment, **92**(1): 51-60.

Wu, P., Kazys, R. and Stepinski, T. (1996). "Analysis of the numerically implemented angular spectrum approach based on the evaluation of two-dimensional acoustic fields. Part I. Errors due to the discrete Fourier transform and discretization." The Journal of the Acoustical Society of America, **99**(3): 1339-1348.

Wu, P., Kazys, R. and Stepinski, T. (1997). "Optimal selection of parameters for the angular spectrum approach to numerically evaluate acoustic fields." The Journal of the Acoustical Society of America, **101**(1): 125-134.

Xiong, L. L., Hwang, J. H., Huang, X. B., Yao, S. S., He, C. J., Ge, X. H., Ge, H. Y. and Wang, X. F. (2009). "Early clinical experience using high intensity focused ultrasound for palliation of inoperable pancreatic cancer." Journal of the Pancreas, **10**(2): 123-129.

Zemanek, J. (1971). "Beam Behavior within the Nearfield of a Vibrating Piston." The Journal of the Acoustical Society of America, **49**(1B): 181-191.

Zemp, R. J., Tavakkoli, J. and Cobbold, R. S. C. (2003). "Modeling of nonlinear ultrasound propagation in tissue from array transducers." The Journal of the Acoustical Society of America, **113**(1): 139-152.

Zeng, X. and McGough, R. J. (2008). "Evaluation of the angular spectrum approach for simulations of near-field pressures." The Journal of the Acoustical Society of America, **123**(1): 68-76.

Zeng, X. J., Li, J. and McGough, R. J. (2010). "A waveform diversity method for optimizing 3-d power depositions generated by ultrasound phased arrays." IEEE Transactions on Bio-medical Engineering, **57**(1): 41-47.

Zippel, D. B. and Papa, M. Z. (2005). "The use of MR imaging guided focused ultrasound in breast cancer patients; a preliminary phase one study and review." Breast Cancer, **12**(1): 32-38.